Marcus Michael Spitz, BSc

Flow component characterization of a complex karst spring

Application of natural and artificial tracers at the example of the Etzbach-Spring, Johnsbachtal

MASTER'S THESIS

to achieve the university degree of

Master of Science

Master's degree programme: Earth Sciences

submitted to

Graz University of Technology

Supervisor

Ass.-Prof. Mag. Dr. Gerfried Winkler

Institute of Earth Sciences

2nd Supervisor

Univ.-Prof. Dr. rer. nat. Martin Dietzel

Graz, 10/2016

AFFIDAVIT

I declare that I have authored this thesis independently, that I have not used other than the declared sources/resources, and that I have explicitly indicated all material, which has been quoted either literally or by content from the sources used. The text document uploaded to TUGRAZonline is identical to the present master‘s thesis dissertation.

Date	Marcus Spitz

ACKNOWLEDGEMENTS

I want to thank Gerfried Winkler for the offer to work at the following topic as well as the continued support during fieldwork and the later (quite extended) period of theoretical work, and Martin Dietzel for the assistance concerning the chemical details of this work.

Furthermore, I would like to thank Christian Steinbauer for the fun time during our fieldtrips and the helping hand during the fieldwork.

All the field- and theoretical work asides this whole thesis would not have been possible without the support of all the staff from Joanneum Research with Albrecht Leis and Sabine Lindbichler leading the way, as well as the staff from the TU Graz, Maria Hierz and Andrea Wolf.

After all, I am grateful for my time studying in Graz and all the amazing and cheerful people I had the advantage to meet during this time. Thank you Mirjam, Daniel, Kathi, Paul, Vera, Eva, Lukas, Stephan, and all the other people not mentioned here!

Abstract

Located at the foot of a karstified carbonate rock formation the Etzbach spring surfaces as a combination of multiple outlets within a 20 m wide section. Coming from the margins, the surfacing water flows into the subjacent central depression, a water filled basin with both diffuse and specific outflow. Whereas the discharge of most karst springs is described to be temporally dominated by either matrix or conduit flow, this spring displays both flow components permanently at different outlets. The autogenic matrix flow is represented by the marginal outlets, mostly affiliated with the carbonate rocks directly above the Etzbach spring. Conduit flow is bound to allogenic recharge and cirques, e.g. the Bärenkar cirque, above the carbonate rocks, especially during snow melt or heavy precipitation events. The superficial runoff from the Bärenkar cirque, geologically built up by porphyroid, infiltrates into the subsurface as soon as it reaches the carbonate rocks. From the point of infiltration, the cirque runoff flows approximately 1 km within the carbonate rocks until resurfacing at the Etzbach spring. Multiple uranin tracer tests have verified this hydrological connection. Applying the formula from Clark (2015), the $\delta\ ^{13}C_{DIC}$ value and the HCO_3 concentration can be utilized to calculate the mixing fractions of matrix and conduit flow in the sampled spring waters. Although the samples from the margin-basin transition are strongly influenced by matrix system water, the aggregate Etzbach spring discharge is dominated by the conduit system component. This overall conduit-dominance, even during low flow conditions, indirectly displays the ancillary input of the diffuse system to the overall composition.

1 | Introduction

During the 1980's an intensive mapping of springs and water reservoirs in the Eisenerzer Alpen was conducted within a federal cooperation of the Austrian Government. The project "Erfassung der Wasserreserven in den Eisenerzer Alpen" (Probst 1993) included the area of the Johnsbachtal (JBT) in the south of the Gesäuse National Park (s. Figure 1-1). As part of this project the largest spring in means of discharge, the Etzbach spring (EBS), was documented, including measurements of electric conductivity (EC), temperature and discharge rates. Although the EBS was mentioned to be of interest for water supply purposes, no further actions were undertaken (Probst 1993).

With the initiation of a "long-term, interdisciplinary cooperation platform in upper Styria" in 2009 a research project related to the JBT was initialized. Answering several key research questions requires the combined effort of multiple disciplines (natural, social, and engineering sciences). One of these questions addresses the recharge and discharge dynamics of the karst aquifers in the region (Strasser et al 2013). Thus, detailed investigations of the largest spring are essential for a better understanding of the recharge and discharge dynamics. Within the framework of the project additional measurements at the EBS started.

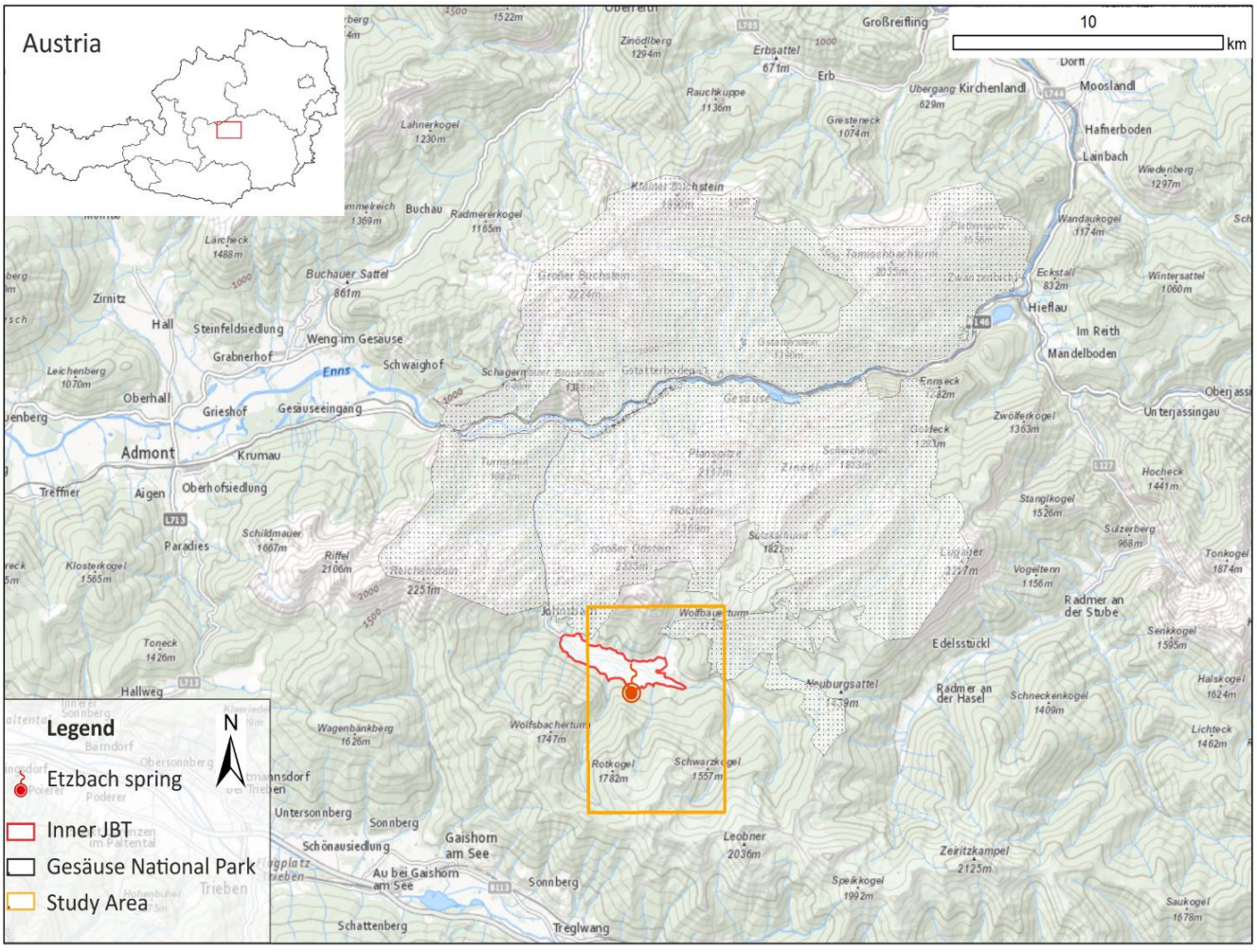

Figure 1-1: Regional overview of the surroundings of the study area, including the areas of the Gesäuse National Park (black, dotted), the inner Johnsbachtal (red outline) and the position of the Etzbach spring (red circle). Base map from basemap.at (grey version).

Both projects documented multiple separate spring outlets at the EBS within 10 meters' width, all combining to one creek (Etzbach). When measured at the same time, discharge, pH, temperature, and EC of these outlets vary significantly despite their spatial proximity of a few meters. Seasonal variations of these parameters at karst springs have already been documented multiple times (e.g. Shuster & White 1971, Jacobson & Langmuir 1974, Atkinson 1977, Jawad et al 1986) and have been quantified using different approaches from Ca/Mg ratios, the variation coefficient of hardness or their total solute load.

In general, karst springs are affiliated with a karst system which comprises two different possibilities of water transport (flow components), which can flowingly merge into each other. On the one hand is the matrix or fissured system in which water is transported with slow velocity through small fissures and cracks in the carbonate rock mass. Within this system most of the spring water volume is stored resulting in quite homogeneous, well balanced water properties. On the other hand, the conduit system originated from the ongoing dissolution of carbonate host rock and successive widening of flow channels, capable of transporting water with high velocities. With ongoing connection of flow channels an underground flow network develops, capable of discharging m^3 of water per second. This system is strongly active during and after precipitation events (recharge periods) as its storage capabilities are strongly limited. Karst springs like the EBS mostly occur as overflow springs, surfacing at the transition from carbonate rock to a barrier with significantly lower permeability (LaMoreaux 2001).

This study focuses on the differences between the separable spring outlets representing different flow components at the same time and their characterization to get an idea about the karst system supplying the EBS. Consisting of multiple outlets with different physical-chemical properties, the sampling and analysis of the EBS waters is the first step towards their characterization and classification. Therefor sampling locations were defined at the separate outlets of the EBS including an additional bulk sample. These locations provide a preferably complete coverage of all waters emerging from the EBS.

From November 2014 until September 2015 these locations were sampled in a bimonthly interval with closer steps during snowmelt in April/May. These samplings contained water chemistry analysis (main and trace elements, alkalinity), isotope sampling (carbon/oxygen/deuterium), discharge measurements and field parameter measurements (temperature, EC, pH, oxygen saturation). The collected chemical data will be used to divide the sampled waters into different groups and to assign them different flow component characteristics. Furthermore, the isotopic data will be used to gather information about the evolution of the groundwater (carbon) and their source area related to its altitude (oxygen/deuterium). Chemical and isotopic data will also be correlated with the respective discharge volume to assess the response to a variable yield.

In addition to the chemical characterization, an uranin tracer test was performed in June 2015 in the Bärenkar Creek, a sinking stream close to the topographical catchment area. A potential hydrological connection between the EBS and the Bärenkar can be determined with the evaluation of the uranin tracer test data.

2 | Site description

Geography, Geology and ore deposits

The Johnsbachtal (JBT), which is part of the Gesäuse National Park, is located in Upper Styria, Austria. With elevations ranging between 600-700 m in the valley and summits over 2300 m the JBT is described as a "comparatively small, high Alpine river headwatershed" (Strasser et al. 2013). The upper JBT, where the EBS is located, extents in E-W direction over a length of approximately 4 kilometers.

As shown in Figure 2-1 the area of the JBT is located near the transition from the mesozoic units of the Northern Calcareous Alps (NCA) in the north to the paleozoic Greywacke Zone (GWZ) in the south, separated by a tectonic contact following the E-W extension of the JBT (Figure 2-1). Based on the conodont-stratigraphic results of Schönlaub and Flajs (1980) the tectonic units are classified as followed: The three important tectonic units in this area are the Blasseneck porphyroid as the basement, the ore-bearing carbonate rocks, and the Werfen formations as hanging units, of ordovician, devonian and triassic age respectively. Whereas the porphyroid and the ore bearing carbonate rocks are both part of the GWZ, the Werfen formation is the basement of the NCA.

The porphyroid is a product of probably subaeric volcanic activity, as pyroclastic lava poured onto the ocean floor (Schönlaub 1982). The ignimbrite is characterized by a fine grained structure with regular quartz and feldspar phenocrysts with an overall thickness of approximately 500 - 600 m in the study area. With a thickness of 400 – 500 m, the overlaying carbonate rocks inhibit ore deposits. They appear as massive, fine grained carbonate rocks with little to no lamination present (Hießleitner 1935 and 1958, Schönlaub 1982). At the transition from GWZ to NCA the ore-bearing carbonate rocks pass into breccia and schists of the Werfen formation. These units are overlain by limestones of the Werfen strata with a thickness of 300 m. Further north more massive carbonate units of the NCA, like the Wetterstein and Dachstein formation, occur (Hießleitner 1935, Mandl 2000).

The tectonics of the region are intensely studied at the ore mining deposits of the Erzberg near Eisenerz. These deposits are located 20 km east of the JBT and can also be applied to this area. Two tectonic phases have to be differentiated, the older variscan orogeny with a major role during the formation of the GWZ-related units, and the alpine orogeny. During the variscan orogeny the thickness of the ore-bearing carbonate rock sequence was tectonically doubled. Afterwards, the Werfen formation was built up transgressively upon the carbonate rocks of the GWZ. As a result of the northward drift of the African continent during the alpine orogeny the units of the GWZ underwent a second alteration, causing the tilting of the GWZ units (Schönlaub 1982).

As the spring being located in the southern part of the upper JBT, the supposed catchment area would mainly be dominated by ore-bearing carbonate rocks and porphyroids. The ore-bearing carbonate rocks are dipping towards NNE with an average angle of 50° and show signs of strong karstification. One example for the extensive carbonate dissolution is the Odlstein cave at 1085 m right in the centre of the topographical catchment (s. Figure 2-1). Another indication of the karstification is a sinking stream approximately 1 km east of the EBS. The sinking stream drains the area of the Bärenkar and its creek is characterized by seasonal discharge fluctuations. This creek will henceforth be referred to as Bärenkar Creek (BKC).

Iron and copper mining (Ankerite, Siderite and Chalcopyrite) was common in the JVC and neighbouring valleys (Klausgraben, Finstergraben) until the beginning of the 20th century (Redlich 1920 and 1922, Hießleitner 1935). More important and popular is the ore mining at the Erzberg near Eisenerz where Ankerite (10-18 % Fe) and Siderite (38-41 % Fe) are still being exploited.

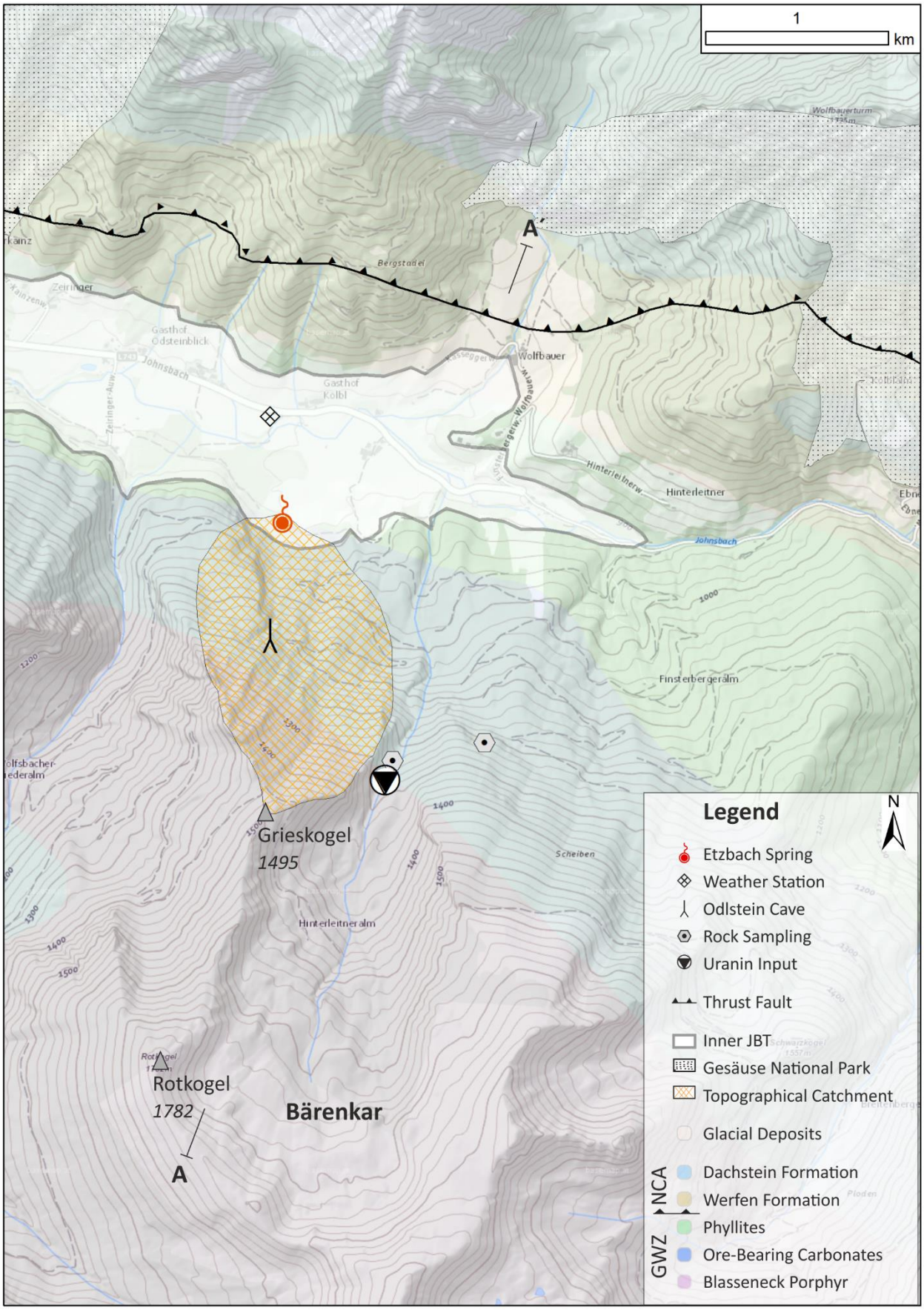

Figure 2-1: Geological overview of the Johnsbachtal in the vicinity of the Etzbach spring in Upper Styria, Austria (yellow rectangle in Figure 1-1).

The origin of the ore deposits is still not definitely resolved, but most commonly supposed of an epigenetic metasomatism during which iron-rich hydrothermal solutions altered the fissured carbonate rocks producing Ankerite and Siderite.

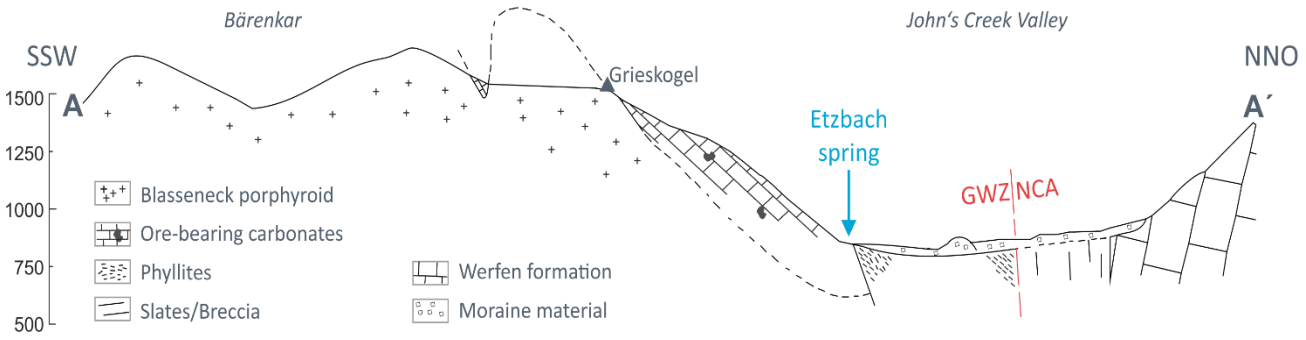

Figure 2-2: Geological profile A-A' (s.) of the JBT in SSW-NNE direction. Clearly visible is the transition from the Greywacke Zone units to the Northern Calcareous Alps in the north (red line). Furthermore, the dipping of the ore-bearing carbonate rocks (approximately 50°) towards NNE is illustrated (Edited after Hießleitner 1935).

Quaternary development

In the late quaternary period glacial development was essential for the present-day appearance of the JBT. During the Riss glaciation all of the JBT and its surroundings were ice-covered. With the end of the glacial periods the retreating glaciers left unstable hillslopes and rock mass movements began to strongly influence the morphology of the valley. One crucial event was the deposition of an enormous debris flow at a narrow point of the valley between the mountains Ödstein and Ahorneck at the transition from the lower to the upper JBT. As a result, the John's Creek was dammed and the transported fluviatile sediments deposited, therefore filling the valley bottom (Lieb 2008). Due to the reduced flow velocity in the water storage area the sedimentation of fine-grained particles was possible.

Hydroclimatology

With elevations above 700 m the upper JBT displays a typical alpine climate with strongly varying temperatures, long winters and moderate precipitation. At the automatic weather station Kölblwiese located 200 m north of the EBS at 860 m (s. Figure 2-1), the mean annual temperature and precipitation for the years 2014 and 2015 are 7.0 °C and 933 mm respectively. As part of the cooperation platform in upper Styria (as mentioned in the introduction) the JBT and its surroundings are equipped with twelve weather stations mostly operated by the University of Graz. The location and specification of all weather stations in the vicinity of the JBT are listed in Strasser et al (2013).

The Etzbach spring

According to Probst (1993) the EBS (Coordinates (UTM 33N): 470,719 / 5,263,960 and the reference number 533/1) is the largest spring in the JBT with discharge rates varying between 50 and 500 l/s. It is located at the southern mountain foot of the upper JBT. The catchment area (Figure 2-1: orange mesh) of the EBS, as determined by the topographical map, covers an area of roughly 0.62 km^2 with the highest point being the Grieskogel at 1495 m asl. The surrounding area can be described as a mixture of productive land, wet meadows on the valley bottom and woodland with forest roads on the hillside of which

one of them directly crosses the area of the EBS. The swampy area surrounding the EBS indicates a very shallow groundwater level in the valley sediments.

As shown in Figure 2-4 the shape of the EBS is a water-filled basin with a diameter of approximately 10 meters with additional definable outlets to both sides of the center extending the width of the spring to 20 meter. The basin can be described as an area of diffuse outflow with several main outlets with varying position depending on the changing hydraulic conditions of the system. These observations seem to fit the characteristics of an overflow spring.

The outlets (#00, #01 and #08) to both sides are clearly separable and slightly elevated compared to the basin itself. Depending on the discharge rates the water level and the area covered with water fluctuates making it difficult to ensure discrete sampling locations. To conquer the problem of varying sampling locations, the "outlets" #02 - #07 had to be defined, based on the present flow situation in November 2014. The definition of these outlets included criteria such as statistical distribution over the whole area, adequate sampling depths and minor to no influence by the forest road. Iron bars labelled with the respective sampling location number were used to mark the locations (see Figure 2-3).

Figure 2-3: Sampling location marked with an iron bar.

As the number of sampling locations stays within single digits, they will in the later be referred to as #0 - #9.

Sampling locations

#0

Being located at the left side of the spring, the outlet itself is a small pool next to the forest road, which nearly falls dry during periods of low discharge. Samples from the original location will afterwards be addressed by #0 "pool" (sampled during high discharge conditions) and the alternative samples (during low discharge conditions) by their sampling location #0 "road", which consists of upwelling water on the forest road directly below the original #0 pool. Both the pool itself as well as the water flowing onto the forest road show a red-brown coloration indicating some iron precipitation, which disappears while flowing towards the central depression. This outlet has the orange color code throughout this work.

#1

Similar to #0 this outlet appears as a pool located next to the forest road without falling dry during low discharge conditions. The outlet drains diffusely onto the road, combines with waters from outlet #0 and flows into the basin. This outlet has the purple color code throughout this work.

#2-#7

These locations are all located in the central basin at the beginning of the EBS. They are primarily influence by the spring discharge and the resulting variations of the water level in the basin, causing #3 as the upper most to fall dry seasonally. No replacement is viable because of the close proximity to #2 and #4. The sum of all six samples is later on referred to as "basin samples". These outlets have the white color code throughout this work.

#8

This outlet is, similar to #0 and #1, located at the forest road over which its discharge reaches the basin. It is the only location with an isolated and clearly distinguishable outlet. This outlet has the grey color code throughout this work.

#9

Whereas the other 9 locations resemble sites where water surfaces, this location provides a bulk sample of the cumulative spring discharge. This outlet has the blue color code throughout this work.

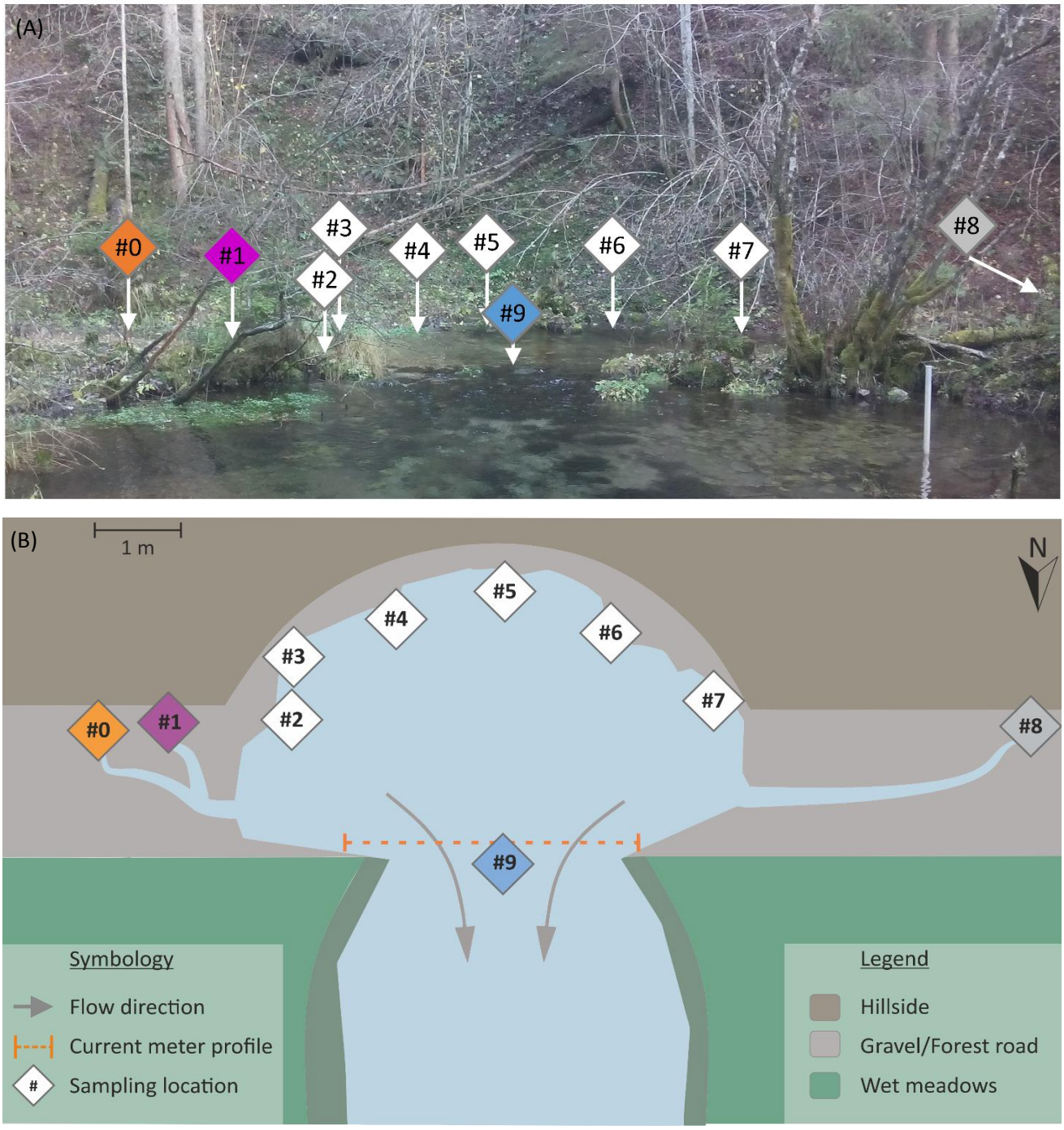

Figure 2-4: Overview of the Etzbach Spring. (A) Picture of the Etzbach Spring taken in November 2014 bevor the sampling locations were marked with iron bars. Approximate position of all sampling locations is visualized. Direction of view is to the south. (B) Schematic aerial view of the Etzbach Spring showing the distribution of the sampling locations and the profile where the current meter discharge measurements were performed.

3 | Sampling and methodology

Fieldwork

In the period from October 2014 until September 2015 multiple fieldtrips for water sampling, discharge and field parameter measurements and tracer tests were performed. 87 water samples were taken during 10 fieldtrips to the EBS whereby one fieldtrip (09.02.2015) only yielded discharge measurements because of heavy snowfall in February and will therefore not be mentioned explicitly. As shown in Figure 2-4 the spring discharge was measured in 3 meters' distance from the spring outlets (orange dashed line) using a current meter (SEBA Mini current meter type M1, SEBA Signal Counter Z6). Within the framework of this research, an uranin tracer test was performed in June 2015 using a flow-through field fluorimeter (GGUN-FL, Schnegg 2003). Previously acquired tracer test data from the years 2013 and 2014 have also been provided and were analyzed, too. The ADM model by Rausch et al. (2002) was used to analyze the tracer test data.

The field parameters water temperature (°C) and electric conductivity (µS/cm) were measured with a TetraCon 325 probe, and pH was measured with a WTW SenTix41 probe, both connected to a WTW pH/Cond 3320. Standard buffer solutions of pH 4, 7 and 10 (Merck) have been used for calibration. The water samples were filtrated in the field using 0.45 µm membrane filters (cellulose acetate) and stored in 250 ml gas-tight borosilicate glass bottles (not acidified) and in 50 ml high density polyethylene bottles (acidified with suprapure HNO_3 to achieve a 2 % HNO_3 solution). The gas tight vials (10 ml) used for carbon isotope analysis were flushed with helium gas and pre-acidified with six droplets of phosphoric acid. 1 ml of solution was injected into the vial with a syringe.

Spring discharge

A direct discharge measurement at the individual spring outlets #0 - #8 was not possible because of the ground-level outflow of the water, making visual estimation the only possibility for data acquisition. Outlet #8 is the only location where water runs out separately, without interference from any other discharge component (problem of the basin samples), and as an actual outflow and not diffusely seeping onto the surface as at #0 and #1. Firstly, the discharge in l/s of #8 was visually estimated. Secondly, the discharge of the remaining eight outlets was estimated as a relative fraction or multiple of the #8 discharge. The obtained proportions were transformed into percent values, making it possible to calculate discharge values for #0 - #7 form the discharge in l/s of #8. The greater part of the discharge surfaces unmeasurable in the pool. The cumulative discharge value (outlets and pool outflow) can be measured at #9 providing a rough estimates of the pool outflow by subtracting the cumulative outlet flow from the total discharge at #9.

Fluid phases (hydrochemistry and isotopes)

All samples were stored at about 5° C until analysis. Carbonate alkalinity was measured the day after sampling with a Schott TitroLine alpha plus titrator using a 0.02 M HCl solution. Anions in solution were determined with an ion chromatography (IC) unit (Dionex IC S 3000, IonPac® AS19 and CS16 column, analytical error < 3%). Cations and dissolved silica were measured with a Perkin Elmer OPTIMA 8300 DV ICP-OES (analytical error < 5%). Oxygen and deuterium isotopic composition of calcite was analyzed using a DELTA^{plus} XP Mass Spectrometer and the phosphoric acid method (Révész & Landwehr (2002), Spötl & Vennemann (2003)). All isotopic values are expressed versus the VSMOW (Vienna Standard Mean Ocean Water) standard.

Calculation of saturation indices and ion activities as well as data plotting was realized with Aquachem 2014.1 and the integrated Phreeqc extension. Hydrogen, Oxygen and Carbon isotopes are expressed as

$$\delta = \left(\frac{R_{sample}}{R_{standard}} - 1 \right) * 1000$$

where R is the isotope ratio measured in a sample and the respective standard used to express the isotope data. For hydrogen and oxygen, the Vienna Standard Mean Ocean Water standard (VSMOW) and for carbon the Vienna Pee Dee Belemnite standard (VPDB) is used.

Solid phases

Two solid samples of the host rock were taken in the field (see Figure 2-1 for locations) for the comparison of host rock and spring water composition. For the mineralogical characterization a powder X-ray diffraction (XRD) analysis using a PANalytical X'Pert PRO diffractometer with a Co-Kα x-ray radiation source (40 mA, 40 kV) and a 2Θ-range from 4 to 85° with a step size of 0.008° 2Θ and counting time of 40s per step was applied. PANalytical Highscore Plus software was utilized to identify mineral phase components. Carbon, oxygen and deuterium isotopic composition of the water samples was analyzed using a DELTA^{plus} XP Mass Spectrometer.

Precipitation

Two weather stations were utilized to acquire data for precipitation values and water isotopes data. Precipitation data was taken from the before mentioned weather station “Kölblwiese”, located 200 m north of the EBS and operated by the WegenerNet (http://www.bogner-lehner.net/xeis_datenportal.php (2015)) of the University of Graz. Water isotopes data was acquired from the nearest weather station with a similar elevation range as the surroundings of the EBS. Being located 34 km west of the JBT the station Planneralm at 1605 m asl is suited to provide compatible data. The station is part of the Umweltbundesamt water isotopes monitoring system for Austria (UBA - http://www.umweltbundesamt.at/ (2016)).

4 | Results

Discharge

Every fieldtrip featured the measurement of the total spring discharge as well as a visual estimation at the defined outlets. The goal was to get an idea about the discharge proportions of the single outlets contributing to the total spring discharge. Table 4-1 summarizes these estimations for the fieldtrips from March until September 2015, including the discharge values from the current meter measurements at #9. The outlets #0/#1 as well as #2/#3 are combined in this overview because it is not possible to separate their fractions from one another. Although these values only serve as a very rough estimation, the difference between the combined discharge of the defined outlets (#0-#8) and the total discharge (current meter measurement) is striking. Only 10 – 20 % of the total discharge is originating from the sampling locations at the rim of the EBS.

*Table 4-1: Estimated (%) and calculated (l/s) discharge values for the outlets #0 - #8. The discharge value for #9 comes from the current meter measurements. The estimated discharge volume for #8 is shaded in grey. *The discharge value of the fieldtrip in June was measured 50 m downstream at a new gauging station of the Hydrographic Service of Styria.*

	24.3.15		14.4.15		10.5.15		19.5.15		8.6.15		12.7.15		10.9.15	
Discharge	(%)	(l/s)	(%)	(l/s)	(%)	(l/s)	(%)	(l/s)	(%)	(l/s)	(%)	(l/s)	(%)	(l/s)
#0 + #1	30	2.4	7	3.6	7	3.2	13	3.0	17	3.6	14	1.9	15	2.3
#2 + #3	20	1.6	17	9.0	21	9.5	26	6.0	33	7.2	21	2.9	19	3.0
#4	5	0.4	13	7.2	19	8.4	13	3.0	8	1.8	10	1.3	7	1.1
#5	10	0.8	17	9.0	24	10.5	26	6.0	17	3.6	18	2.4	19	3.0
#6	8	0.6	20	10.8	14	6.3	6	1.4	8	1.8	14	1.9	16	2.5
#7	7	0.6	23	12.6	10	4.2	9	2.0	8	1.8	11	1.4	13	2.1
#8	20	1.6	3	1.8	5	2.1	9	2.0	8	1.8	12	1.6	10	1.6
Sum	100	8.0	100	54.0	100	44.1	100	23.4	100	21.6	100	13.4	100	15.5
#9		41		372		419		225		*157		78		
Sum/#9		**0.20**		**0.15**		**0.11**		**0.10**		**0.14**		**0.17**		

Field measurements

All data gathered are shown in the appendix in Table A-1 - A-9. An overview of the value range of the obtained water chemistry data is presented in Table 4-2. The values represent the mean value and the respective standard deviation of all samples taken on the given date from November 2014 until September 2015. Electric conductivity (EC) values range between 221 and 321 µS/cm, water temperature (T) (6.2°C - 6.9°C) is below to the annual mean temperature of 7.0 °C in the valley. Ranging between 7.7 and 7.8, the pH-values show a nearly constant trend of slightly increased values, which is not surprising considering the carbonate host rock and its dissolution. The discharge values are ranging between 41 - 419 l/s at the outlet of the spring.

At first sight the correlation of EC/temperature and discharge is identifiable. The lowest (41 l/s) and highest (419 l/s) discharge values were measured in March and May respectively. At the same datum, the reverse extreme values for EC and temperature were recorded.

Table 4-2: Overview for all water chemistry samplings from November 2014 to September 2015. Values given represent the mean value and their standard deviation of all samples taken at the respective datum.

Sampling	1		2		3		4		5		6		7		8		9	
Date	10.11.14		19.12.14		24.03.15		16.04.15		10.05.15		19.05.15		08.06.15		12.07.15		10.09.15	
Field data																		
El. cond. (µS/cm)	257	± 82	286	± 70	321	± 62	264	± 75	221	± 92	244	± 85	276	± 82	297	± 64	278	± 66
Temperature (°C)	6.7	± 0.3	6.6	± 0.8	6.9	± 0.2	6.5	± 0.4	6.2	± 0.7	6.6	± 0.6	6.8	± 0.5	6.9	± 0.4	6.8	± 0.2
pH-Value (-)	7.8	± 0.1	7.7	± 0.1	7.7	± 0.1	7.8	± 0.2	7.8	± 0.2	7.8	± 0.2	7.8	± 0.1	7.8	± 0.1	7.8	± 0.1
$O_{2\,(aq)}$ (mg/l)	8.8	± 3.1	9.0	± 1.6									9.8	± 1.0	9.6	± 0.8		
Discharge																		
Spring (l/s)			51		41		372		419		225		50		78			
Isotopes																		
$\delta\,^{18}O$ (‰ VSMOW)					-11.4	± 0.1	-11.8	± 0.3	-12.0	± 0.4	-11.8	± 0.3	-11.7	± 0.2	-11.6	± 0.1		
$\delta\,^{2}H$ (‰ VSMOW)					-79.6	± 0.7	-83.2	± 1.8	-82.6	± 1.9	-83.3	± 1.6	-82.0	± 0.2	-82.7	± 0.2		
$\delta\,^{13}C_{DIC}$ (‰ VPDB)	-10.8	± 1.2	-11.6	± 1.1			-10.7	± 1.7					-11.1	± 1.0				
Water-Chemistry																		
HCO_3^- (mg/l)	155	± 54	181	± 43	193	± 39	162	± 45	139	± 60	155	± 57	167	± 45	190	± 67	170	± 39
Cl^- (mg/l)	1.2	± 1.4	1.2	± 0.5	1.0	± 0.4	1.0	± 0.6	0.7	± 0.6	1.1	± 0.7	0.9	± 0.5	1.1	± 0.6	1.0	± 0.5
NO_3^- (mg/l)	3.0	± 1.0	3.9	± 0.6	3.3	± 0.3	4.4	± 1.4	3.5	± 1.1	3.0	± 1.0	3.3	± 0.9	3.6	± 0.2	3.6	± 0.8
SO_4^{2-} (mg/l)	8.6	± 6.6	11.3	± 4.8	13.2	± 5.9	6.8	± 7.1	6.1	± 7.1	7.6	± 6.8	9.5	± 5.4	10.6	± 4.8	9.8	± 5.2
Na^+ (mg/l)	1.2	± 0.5	1.6	± 0.4	1.7	± 0.3	1.0	± 0.5	0.9	± 0.4	1.3	± 0.5	1.4	± 0.4	1.4	± 0.3	1.4	± 0.3
K^+ (mg/l)	0.8	± 1.1	0.8	± 0.3	0.9	± 0.2	0.4	± 0.2	0.4	± 0.2	0.5	± 0.2	0.6	± 0.2	0.6	± 0.2	0.5	± 0.1
Mg^{2+} (mg/l)	5.6	± 2.3	7.2	± 2.3	7.7	± 2.2	5.2	± 2.2	4.7	± 2.5	5.0	± 2.4	6.0	± 2.3	6.6	± 2.3	6.5	± 2.2
Ca^{2+} (mg/l)	46	± 15	47	± 9	54	± 11	47	± 12	41	± 17	46	± 16	34	± 5	50	± 10	42	± 4
Fe^{3+} (mg/l)	0.7	± 1.9	0.0	± 0.0	0.0	± 0.0	1.3	± 3.8	1.5	± 4.5	0.8	± 2.3	0.0	± 0.0	0.0	± 0.0	0.0	± 0.0
Si^{4+} (mg/l)	2.6	± 0.4	2.6	± 0.2	2.6	± 0.2	2.1	± 0.5	2.2	± 0.6	2.4	± 0.4	2.5	± 0.2	2.6	± 0.1	2.5	± 0.1
Sr^{2+} (mg/l)	0.1	± 0.1	0.2	± 0.1	0.2	± 0.1	0.1	± 0.1	0.1	± 0.1	0.1	± 0.1	0.1	± 0.1	0.2	± 0.1	0.1	± 0.1

While the overview Table 4-2 is giving an estimate of the water properties, Figure 4-1 and Figure 4-2 offer a more detailed examination of the field parameters. As already mentioned in the introduction, the parameters temperature, EC and pH display a significant variation from outlet to outlet as displayed in Figure 4-1. EC values range from 150 µS/cm to 400 µS/cm, temperature from 5.5 °C to 7.7 °C and the pH from 7.2 to 8.2. Plotting EC versus temperature or pH shows that this variation follows a general trend. Samples with higher temperatures (> 7 °C) also tend to have EC values above 300 µS/cm whereas samples with temperatures below 7 °C correlate with an EC below 300 µS/cm as seen in Figure 4-2 (A). While elevated ion concentrations and temperatures are characteristic of samples from the verge of the basin (outlets #0, #1 and #2), lower temperatures and EC are associated with samples from the spring basin (#2-#7 and #9).

The same trend can be applied to Figure 4-2 (B), with the difference of an inverted correlation in dependence of pH and the presence of four outliers from the general trend. The pH values of these outliers where all measured in #0 “pool”. Even though the EC of ~ 360 µS/cm is similar to the #0 “road” samples, the pH is lower (~ 7.7 vs. < 7.5).

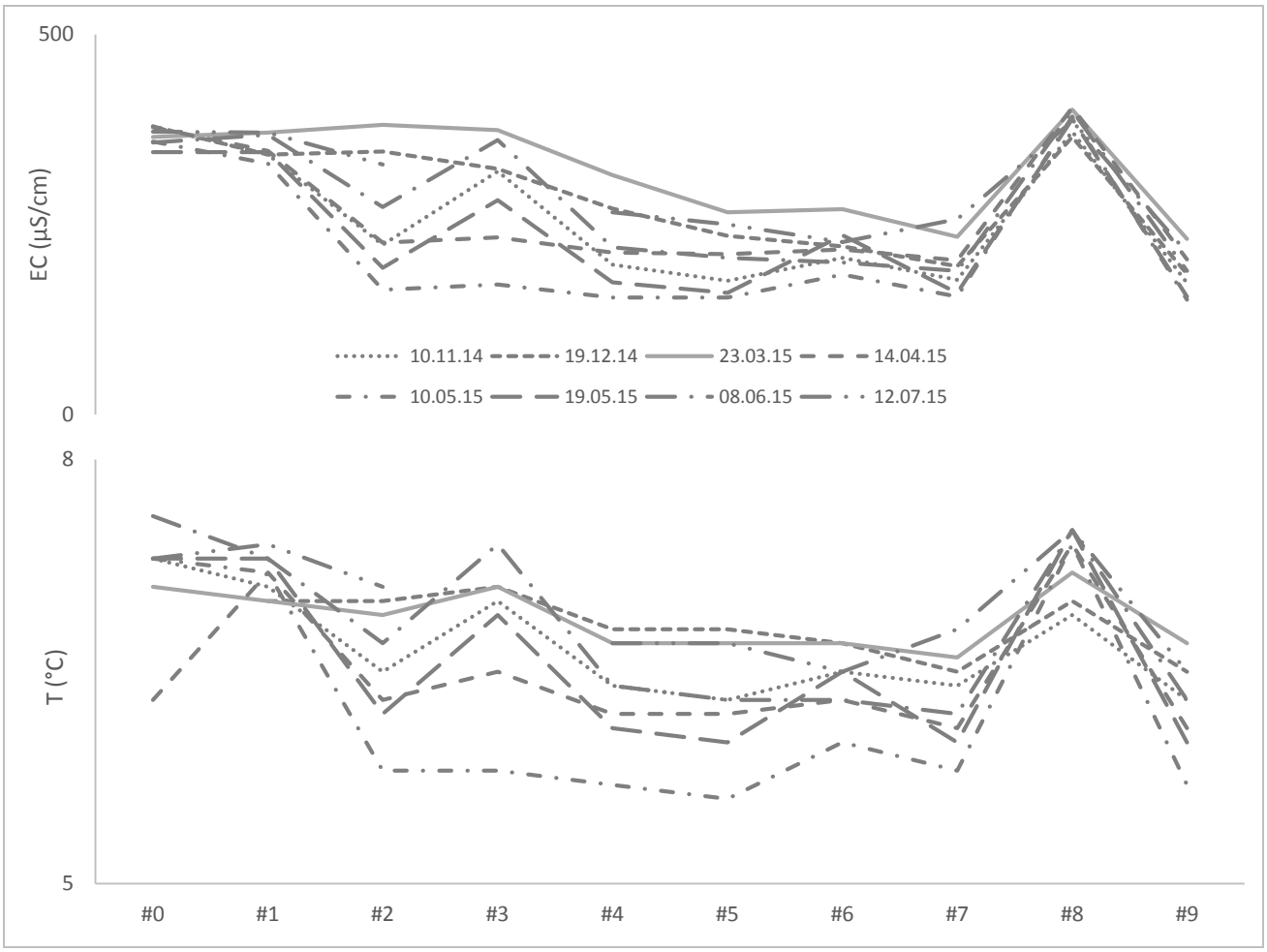

Figure 4-1: Plot of the collected EC (A) and temperature (B) date assorted by outlet location for the fieldtrips from November 2014 until July 2015. Note that the last fieldtrip (10.09.15) is not displayed due to the falling dry of two sampling locations.

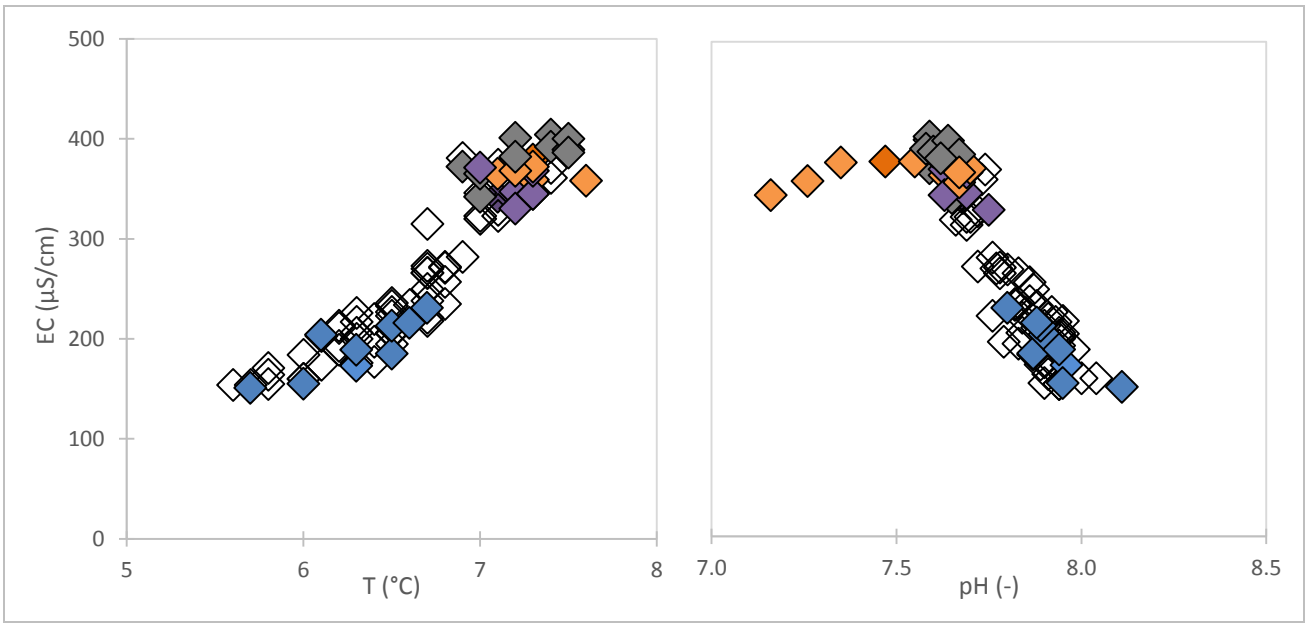

Figure 4-2: Plot of temperature (A) and pH (B) in dependence of the electric conductivity (EC). Color scheme: #0 (orange), #1 (purple), #2-#7 (white), #8 (dark grey), #9 (blue).

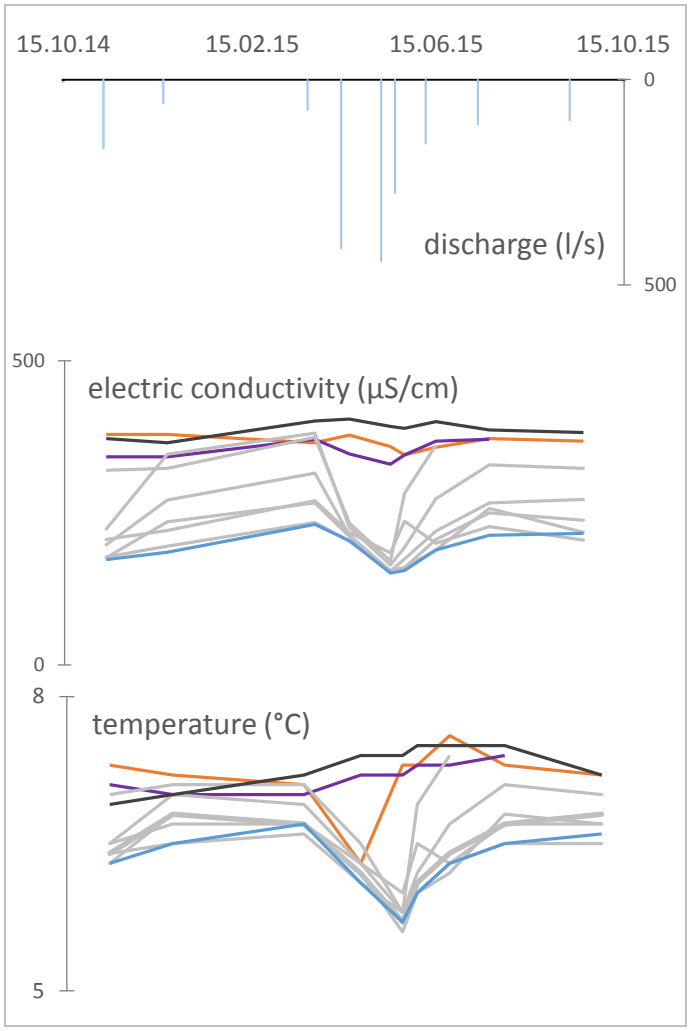

Figure 4-3: Correlation between the spring discharge and the measured field parameters (electric conductivity, temperature and pH-value) from November 2014 – September 2015. Color scheme: #0 (orange), #1 (purple), #2-#7 (light grey), #8 (dark grey), #9 (blue).

Figure 4-3 shows the behavior of discharge, EC, temperature and pH of every single outlet within the observed period from November 2014 to September 2015. For better visibility, the graphs of the outlets #0, #1, #8 and #9 are colored (legend in figure caption). As already mentioned, an increase in spring discharge produces a general decrease of EC and T. However, some sampling locations are more responsive than others. Whereas all basin locations (grey-colored, #2 - #7) and #9 show a similar and strong response signal, the other three (#0, #1 and #8) at the margins of the spring area show little to no decrease of EC and T with an increase of discharge.

The trend for the basin samples during low flow conditions is variable. While some samples follow the trend of the bulk sample #9, others (#2/#3 mostly) tend to the values of the EC and T of those samples from the margin of the EBS.

Water chemistry

The Schoeller and Piper plot in Figure 4-4 display the overall chemical composition for all 87 water samples. As already mentioned before, calcium and bicarbonate dominate, accompanied by magnesium, sulfate, and only minor amounts of sodium/potassium and chloride. Multiplying Mg, Na+K, SO_4 and Cl with a factor of 10 in the piper plot, the samples plot closely in the corner of calcium and carbonate. Therefore, the water type can be described as a Ca-HCO_3 / Ca-Mg-HCO_3 water.

All samples show a similar distribution of main components and a moderate fluctuation with the exception of the three samples in the orange circle in both plots. Again, these three samples were taken at the original #0 pool, showing a significantly lower sulfate concentration compared to all other samples. Furthermore, one sample shows a sodium and chloride excess, this time collected at #9. As this sample being the only one with higher sodium and chloride concentrations and #9 being the first location to be probed, this outlier might be a result of NaCl contamination on the rubber boots.

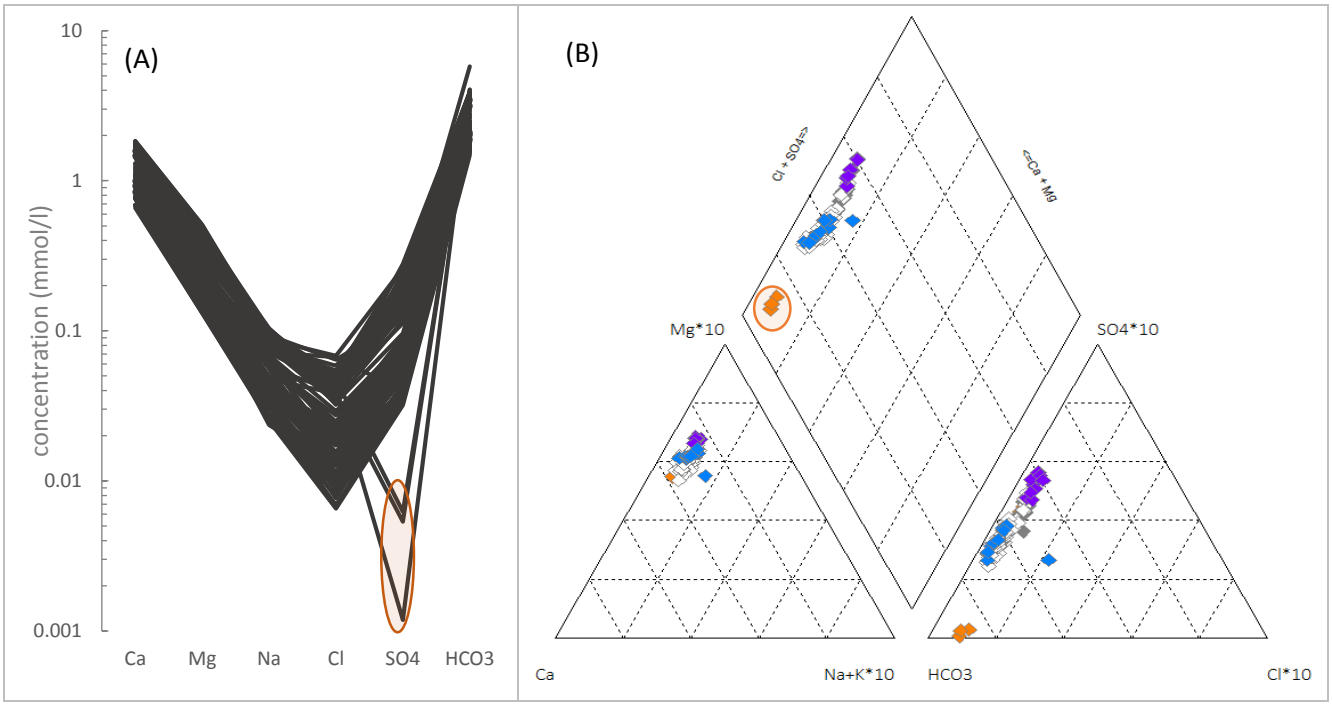

Figure 4-4: (A) Schoeller plot for the main ions of each sample taken. All solutions show a comparably homogeneous composition except three marked with an orange circle. (B) Piper plot for all 87 water samples. Note that the values for magnesium, sodium + potassium, sulfate and chloride are multiplied by a factor of 10 for better resolution. The spring waters can be categorized as a Ca-HCO_3- Ca-Mg-HCO_3 water. Color scheme: #0 (orange), #1 (purple), #2-#7 (white), #8 (dark grey), #9 (blue).

Figure 4-4 gives a rough overview over the chemical composition of the spring water, but Figure 4-5 provides a first more precise look into the chemical characteristics of the EBS water. All three plots in Figure 4-5 reveal a similar distribution of the individual solute concentrations of the outlets in relation to each other. Figure 4-5 (A) displays the distribution of magnesium versus calcium. Samples taken at the sides of the main basin (#0, #1, #8) show generally elevated ion concentrations > 0.3 mmol/l magnesium, compared to samples from the basin (#2-#7). Samples taken from #9 show a similar ionic composition as the basin samples. Compared to #8 the samples from #0 and #1 (close spatial proximity) show slightly lower magnesium concentrations. The strontium and magnesium concentrations shown in Figure 4-5 (B) are characterized by a nearly constant Sr/Mg ratio of 0.0062 for all water samples. Interestingly the #0 “pool” samples plot closer towards the basin samples whereas #0 “road” samples compare with the water chemistry of outlet #1.

Figure 4-5 (C) display a clear separation between the basin waters with low concentrations (blue circle) and the waters from the sides (purple circle). Samples in between these two regimes originate mainly from the outlets #2, #3 and #4, taken during low discharge conditions. The two trend lines show the difference between a perfect 0.5/1 mix of cations and anions whereas the overall trend line displays a slightly higher value of 0.54/1.

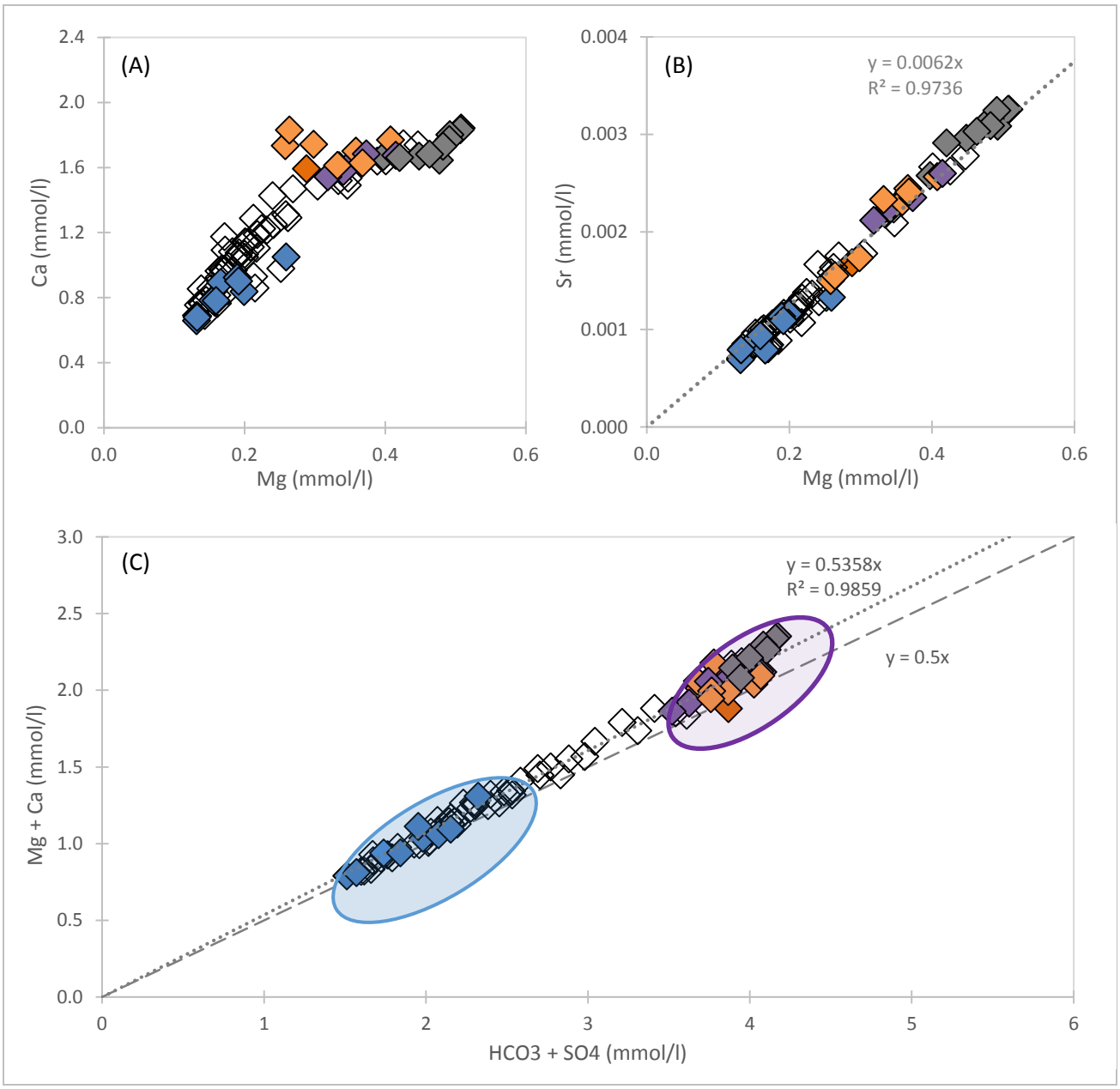

Figure 4-5: Dissolved calcium (A) and strontium (B) as a function of dissolved magnesium. (C) Sum of dissolved magnesium and calcium vs. sum of dissolved bicarbonate and sulfate. Color scheme: #0 (orange), #1 (purple), #2-#7 (white), #8 (dark grey), #9 (blue).

Besides the ionic composition, the partial pressure of CO_2 is an important parameter for a carbonate-rock dominated spring, plotted in Figure 4-6. Outlets located on the verge of the EBS tend to contain larger amounts of CO_2 with higher HCO_3 concentrations and lower pH-values as shown in Figure 4-6 (A) and (B). The four samples of the #0 "pool" show the highest values regarding CO_2 content, whereas the #0 "road" samples are comparable to #1 and #8 waters. Waters from the basin and the bulk sample #9 have the lowest pCO_2 values and trend towards the atmospheric CO_2 pressure of $10^{-3.5}$ kPa

.

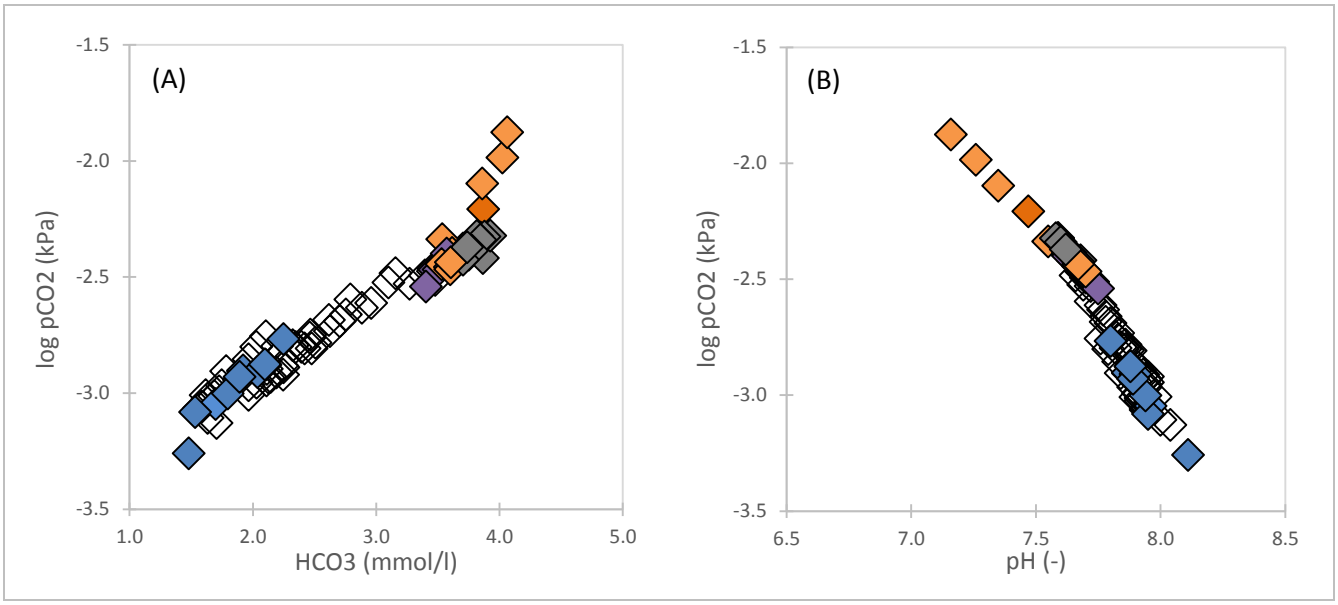

Figure 4-6: Partial pressure of CO_2 in dependence of HCO_3 (A) and pH (B). Color scheme: #0 (orange), #1 (purple), #2-#7 (white), #8 (dark grey), #9 (blue).

All samples taken are near equilibrium regarding the saturation of Calcite as displayed in Figure 4-7 (A). Slight superstation in respect to calcite may result from partial degassing of CO_2. Although being at near equilibrium four groups of solutions are distinguishable - (i) Samples from the verge (#0 "road", #1, #8) are slightly oversaturated regarding calcite, with values ranging from 0.1 to 0.2. While having the same state of saturation, samples from #8 are plotting towards higher sulfate values compared to #0 "pool" and #1 samples. (ii) Basin samples including #9 are in equilibrium or slightly undersaturated state (0.1 to -0.3) with sulfate values < 0.1 mmol/l. While the samples #0 "pool" (iii) have similar saturation indices as the basin samples, their sulfate concentrations are below 0.01 mmol/l. Group (iv) consists of basin solutions from #2, #3 with values from 0.1 to 0.2 and sulfate concentrations > 0.1 mmmol/l, similar to group (i) samples. Figure 4-7 (B) displays a nearly identical sample distribution with the difference of an obvious undersaturation with respect to dolomite in all solutions. The distribution of gypsum saturation index in dependence of sulfate concentration in Figure 4-7 (C) shows an undersaturation with respect to gypsum for all samples with values ranging between -2.0 and -4.5. Obviously, the lower the concentration of sulfate the lower the SI for gypsum gets with the minimum values of #0 "pool" and the maximum values determined by #8 samples.

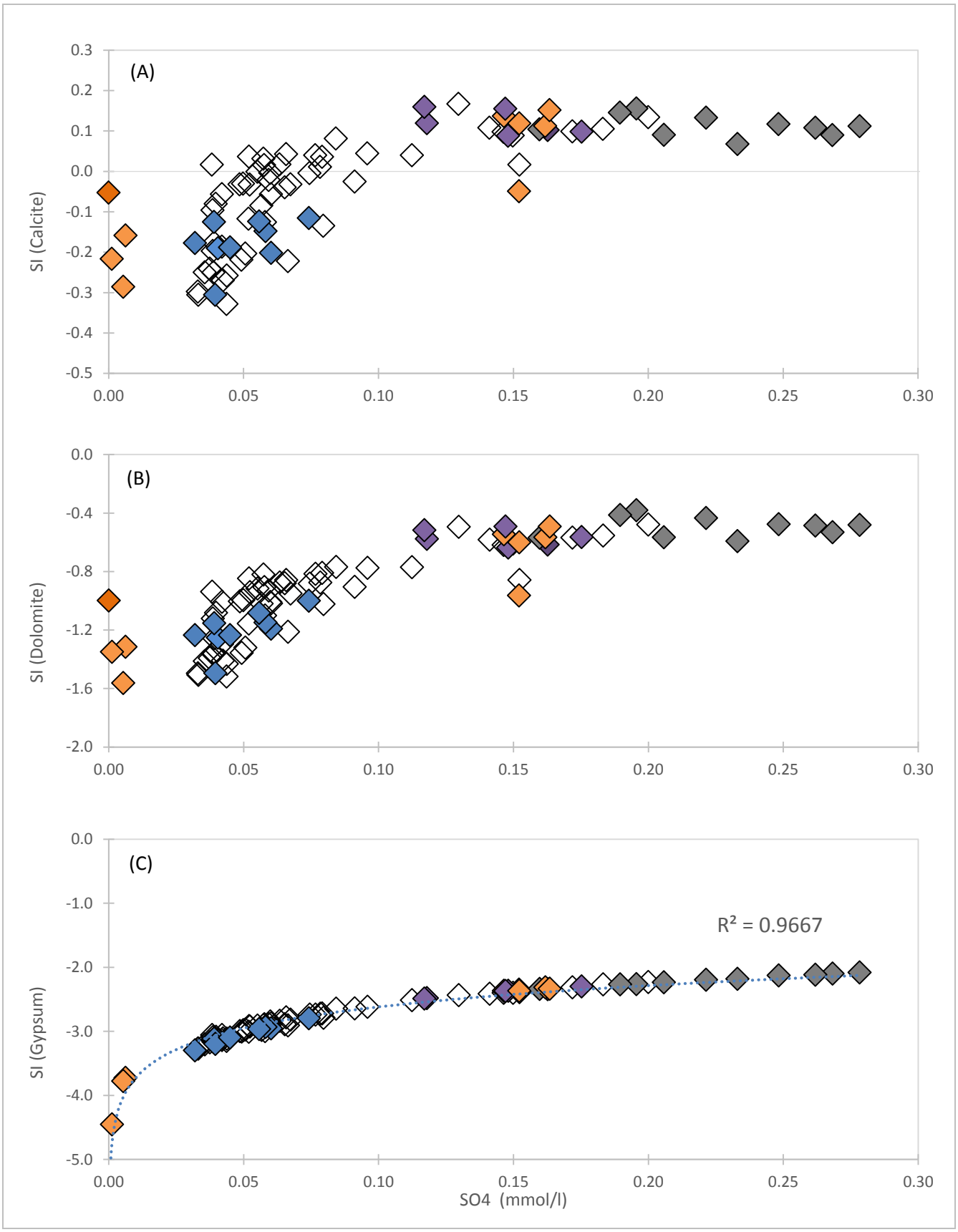

Figure 4-7: Plot of the SI of Calcite (A), Dolomite (B) and Gypsum (C) in relation to the sulfate concentration. The horizontal light grey line in plot (A) indicates the transition from under- to oversaturation of Calcite. Color scheme: #0 (orange), #1 (purple), #2-#7 (white), #8 (dark grey), #9 (blue).

Not only the ionic composition itself is a key feature to the understanding of the EBS system behavior, so is the variation of the solute load over time, presented in Figure 4-8. As already discussed in the chapter “field parameters” the outlets in the basin area (#2 - #7) and the bulk sample #9 respond significantly to an increased discharge. Regarding water chemistry, there also is a response to higher discharge values (April to Mai 2015) but with diverse consequences. For HCO_3, Ca, K, Si and Cl the distinction between basin samples with a higher magnitude of response (lowered ion concentration) and the outlets from the sides (#0, #1, #8) with a comparably stable trend is applicable. Special attention has to be payed to the trend of #0, because the samples taken at the #0 “pool” location coincide with higher discharge values and therefore produce an artificial conformity between ion concentration and discharge and has to be treated with caution.

Figure 4-8 (A) and (B) display a stable trend for samples from #0 “road”, #1 and #8, but with an overall higher magnesium concentration for samples from #8. In contrast to the steady behavior, #8 reacts with slightly increased sulfate values and a time-delayed iron increase to the boosted discharge conditions. The plot for iron concentration is cropped because the four samples from #0 “pool” have significantly higher values (average: 0.1866 mmol/l) compared to the displayed values below 0.0002 mmol/l. During low flow conditions (December-March, June-August), the value range of the basin samples (#2-#7) varies strongly compared to the events of high discharge. During high discharge all samples mostly resemble the #9 bulk value with the exception of the iron content, which follows the inverted trend. The increased discharge is followed by a relatively high iron concentration. The most significant increase can be described for #1 and #3 and a delayed increase at #8.

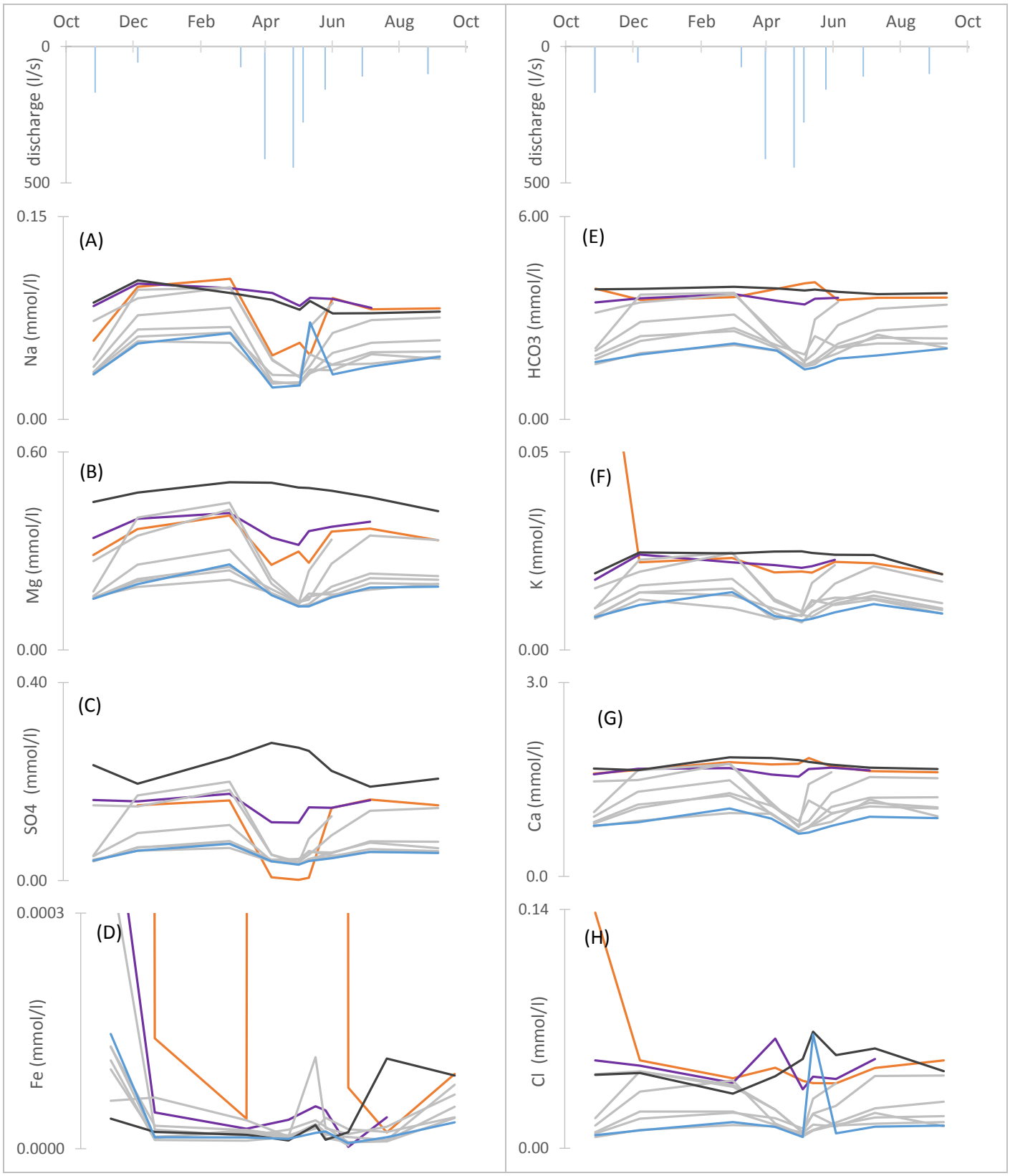

Figure 4-8: Time (October 2014 – October 2015) vs. concentration plots for Na (A), Mg (B), SO_4 (C), Fe (D), HCO_3 (E), K (F), Ca (G) and Cl (H). For comparison, the magnitude of discharge is displayed above. Color scheme: #0 (orange), #1 (purple), #2-#7 (light grey), #8 (dark grey), #9 (blue).

Isotopes

Six fieldtrips featured deuterium (D) and oxygen 18 (^{18}O) isotope sampling, with the data presented in Figure 4-9. In addition to the data gained from the EBS, the D and ^{18}O data from the weather station Planneralm (2009-2013, monthly sampled) was used to create a local meteoric water line (LMWL) with a correlation of $\delta D = 8.26 * \delta^{18}O + 16.1$. Furthermore, the data from the station Planneralm was used to calculate the overall precipitation-weighted average that is represented by the orange box. As seen in Figure 4-9 (A), the EBS water plots in a narrow area between $\delta^{18}O$ values of -11 ‰ to -12.5 ‰. The existing EBS data correlates with the LWML and is close to the value of the weighted average.

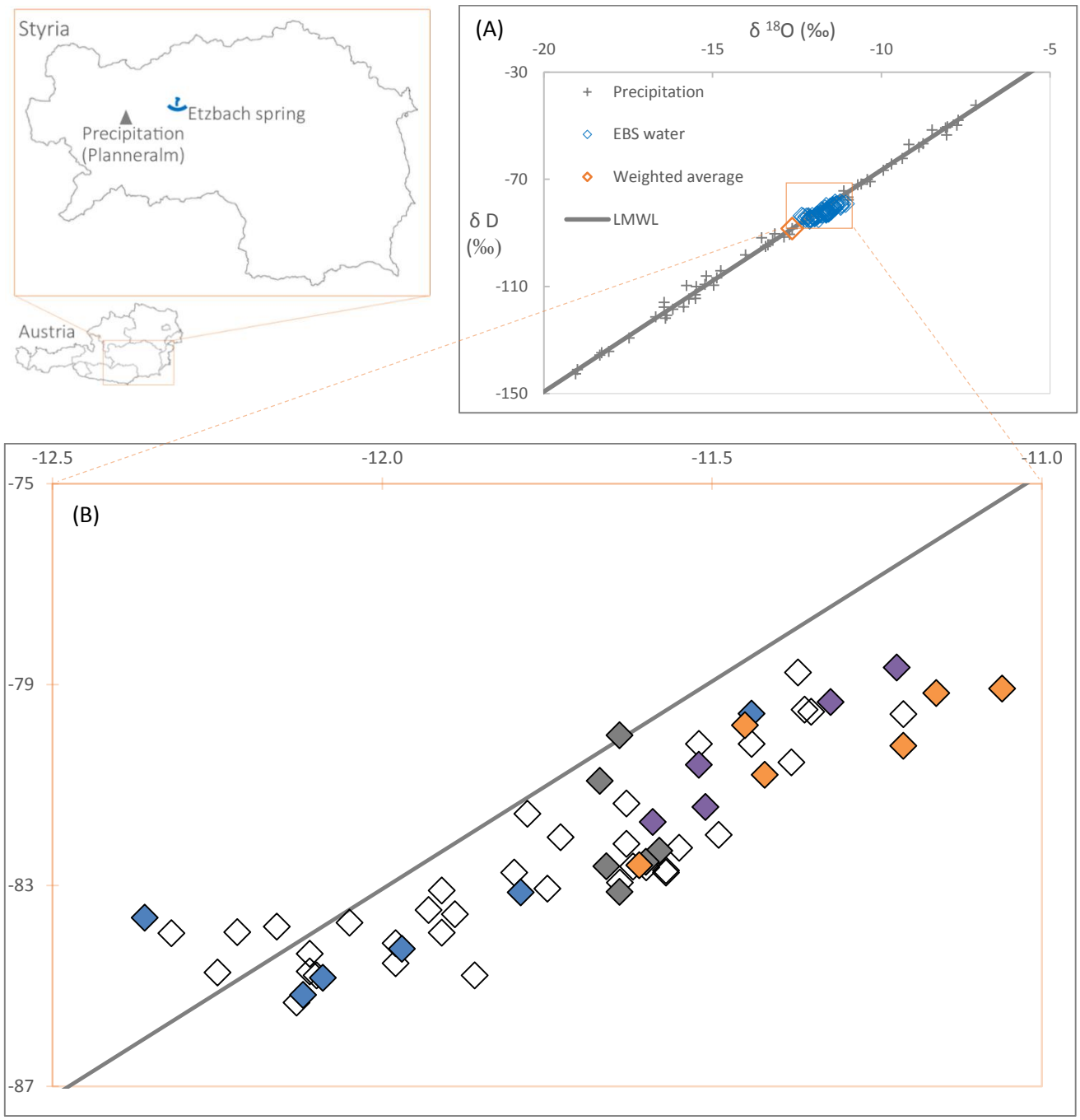

Figure 4-9: Plot of the water isotopes δ D and δ ^{18}O in ‰ relative to VSMOW. The location of the weather station Planneralm in comparison to the EBS is featured in the upper left map. Color scheme: #0 (orange), #1 (purple), #2-#7 (white), #8 (dark grey), #9 (blue).

Figure 4-9 (B) shows the area of the orange rectangle from plot (A) magnified for better resolution of the EBS samples. The previously used color scheme is applied again, showing a similar distribution of the sampled waters along the LMWL. Basin waters (#2 - #7, #9) are characterized by both lighter δ D and δ ^{18}O values whereas the samples from the sides (#0, #1, #8) plot at higher δ D and δ ^{18}O values. The samples of most outlets vary in a range of at least +/- 0.25 ‰ δ ^{18}O, the samples from #8 are within a 0.1 ‰ δ ^{18}O wide window. The range of variation for the individual outlets is presented as a boxplot in Figure A-3, verifying the narrow variation range of #8 and additionally showing a broad spectrum for the other locations.

The value range of δ ^{18}O can be used to approximate the altitudes at which the groundwater recharges. Clark and Fritz (1997) presents multiples studies concerning the gradient of δ ^{18}O decrease per 100 m altitude gained. These values range between -0.10 and -0.50 ‰ for altitudes between 0 – 5000 m asl. Research by Hager & Foelsche (2015) for "Stable isotope composition of precipitation in Austria" stated an altitude effect of 0.19 ‰ · 100^{-1} m. Using a -0.19 ‰ depletion in δ ^{18}O per 100 m altitude gained, a minimum of -12.36 ‰ and a maximum of -11.06 ‰, the resulting altitude difference comes to 684 m. Compared with the generously chosen actual altitude range of 922 m the calculated difference offers a pretty close approximation.

In addition, Figure A-2 (attached in the appendix) displays every fieldtrip individually, including the respective datum, discharge volume and altitude range. Depending on the spring discharge, the sample spread varies significantly. During high discharge events, samples from the basin propagate towards lighter δ ^{18}O values around -12 ‰. A decline of water flow results in the propagation of the basin samples towards values similar to the outlets from the sides of the spring. Low discharge conditions correlate with a small altitude range with a minimum of 116 m relative difference, high discharge events receive their water from an altitude range of up to 553 m relative distance.

At last, Figure 4-10 (A) shows the plot of δ ^{18}O against a conservative element. Strontium was chosen due to the fact that chloride concentrations tended to be flawed by contamination although the distribution of chloride in Figure A-4 (A) is similar to that of strontium. Three groups of samples can be distinguished, (i) the samples from #8, isolated from the rest with the highest strontium/chloride values and little variation in their signal. (ii) Samples from the basin (#2 - #7) including #9 are defined by the lowest concentrations around 0.001 mmol/l strontium but a comparably broad range in their δ ^{18}O signal ranging from -12.5 to -11.25 ‰. Samples with a higher strontium concentration have are plotting towards heavier oxygen isotope values. (iii) In between the two described groups, samples from #0 and #1 and some of #2 and #3 are plotting. These samples (iii) display the greatest variation in strontium concentration ranging from 0.0012 to 0.0028 mmol/l. While the samples from the sides of the EBS are trending towards significantly higher concentrations for strontium and chloride, Figure A-4 (B) shows that the δ ^{18}O vs. silica trend is more like a linear correlation.

Figure 4-10 (B) features the distribution of δ $^{13}C_{DIC}$ as a function of the reversed solute concentration HCO_3. Compared with the conservative tracers discussed before, this plot offers a simplified breakdown. Besides the three outliers (two not so surprisingly from #0 and one from #9), the samples from #0, #1 and #8 plot narrowly together, including the same samples from #2 and #3 of group (iii) in Figure 4-10 (A). For the rest of the basin samples (#2 -#7) and #9 the trend moves away from the narrow plotting samples towards heavier δ $^{13}C_{DIC}$ signatures and lower HCO_3 concentrations. Samples from #7 and #9 mark the lower end of the trend, whereas the samples from #6, #5 and #4 and especially from #3 and #2 trend towards the other extreme marked by #0, #1 and #8.

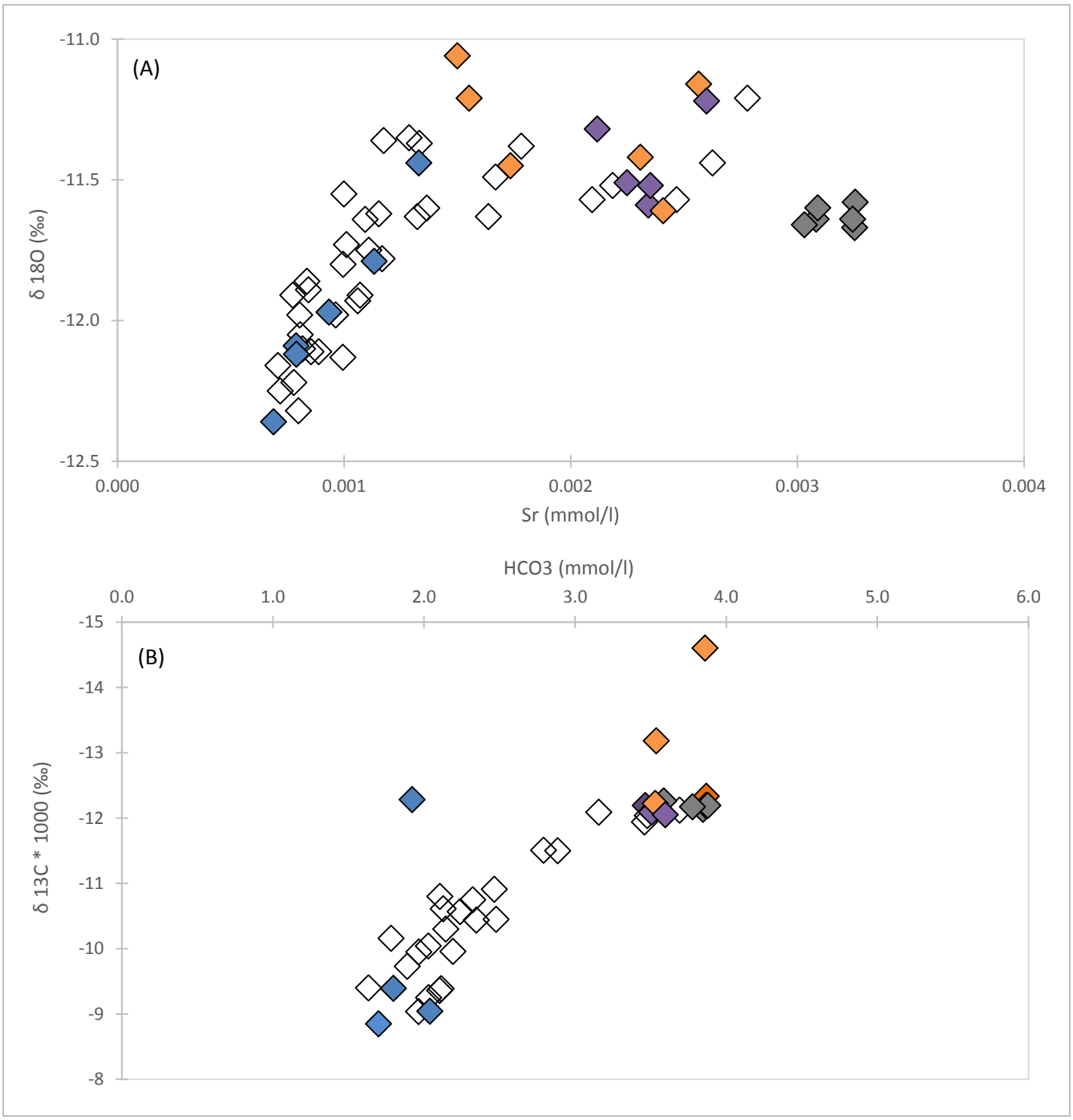

Figure 4-10: (A) Plot of δ ^{18}O in ‰ relative to VSMOW vs. strontium concentration and (B) plot of δ $^{13}C_{DIC}$ in ‰ relative to VPDB vs. the concentration of HCO_3. Note that the y-axis in figure (B) is reversed. Color scheme: #0 (orange), #1 (purple), #2-#7 (white), #8 (dark grey), #9 (blue).

Tracer test data

Three tracer tests were performed in the recharge area of the EBS. At all tests 100g uranin were injected into the Bärenkar Creek (BKC) at the same location marked in Figure 2-1. The Fluorimeter was placed at outlet #2 and the discharge was determined via current meter measurements 50 m downstream at the new gauging station of the Hydrographic Service of Styria. Figure 4-11 shows the results of the performed tracer tests with the breakthrough curve in blue and the recovery-rate in orange. Unfortunately, the Fluorimeter stopped recording after 52 hours due to battery problems in 2013. The recordings for 2014 and 2015 lasted for 300 and 194 hours respectively and are only scaled to 60 hours for better comparison with the test of 2013. The recovery rates range between 40 and 60 % of the initially injected tracer. This value has to be treated with caution, since the discharge value used to calculate the recovery rate was measured 50 m downstream and does not reflect the actual spring discharge and even less the discharge at outlet #2. Additionally, the uncharacteristic increases and sudden drops in the breakthrough curve in 2013 between day 1 and 2 artificially increase the recovery rate.

First of all, a connection between the BKC and the EBS is present and was verified with every tracer test. Furthermore, a good correlation between amount of discharge and first appearance/tracer peak is shown. The more water is discharged at the EBS the faster the water travels within the karst system. While it takes 9.6 h to reach the fluorimeter with a discharge of 157 l/s, the tracer arrives at the spring after 3.1 h with a discharge of 600 l/s. With more water being transported through the karst conduits, the faster the water travels and less mixing occurs. Thus it would be reasonable to assume, that the tracer produces a thinner and more intense peak with increasing discharge and an earlier first appearance. This assumption is correct for the tests from 2015 and 2014 with less tailing and a higher peak intensity. But for 2013 the only accurate feature is the earlier first appearance time. An explanation for the missing of a defined sharp peak might be the enormous discharge volume. As the BKC partially being a sinking stream, heavy precipitation might overextend the volume of water that can infiltrate into the karst system. As a result, excess water (including the injected tracer) would not even infiltrate into the karst system but simply run of as a superficial stream without connection to the EBS.

Using the advection-dispersion model (ADM) by Rausch et al. 2002 to approximate the breakthrough curves a deficit of tracer mass is also encountered. This deficit is partially attributable to the simplicity of this model, since retardation of the tracer cannot be modelled. Thus, the tailing of the breakthrough curve cannot be approximated sufficiently, especially in 2015. But it would be an oversimplification to attribute the difference between injected (100 g) and corrected amount (20 – 37 g) solely to the constraints of the ADM. Again, the behavior of the BKC and a partial superficial runoff could be partly accountable for said differences. The above-mentioned differences in flow velocity could be verified using the ADM. While the tracer travels with an average speed of 0.024 m/s with a discharge of 157 l/s the velocity increases to 0.05 m/s when the discharge is 600 l/s.

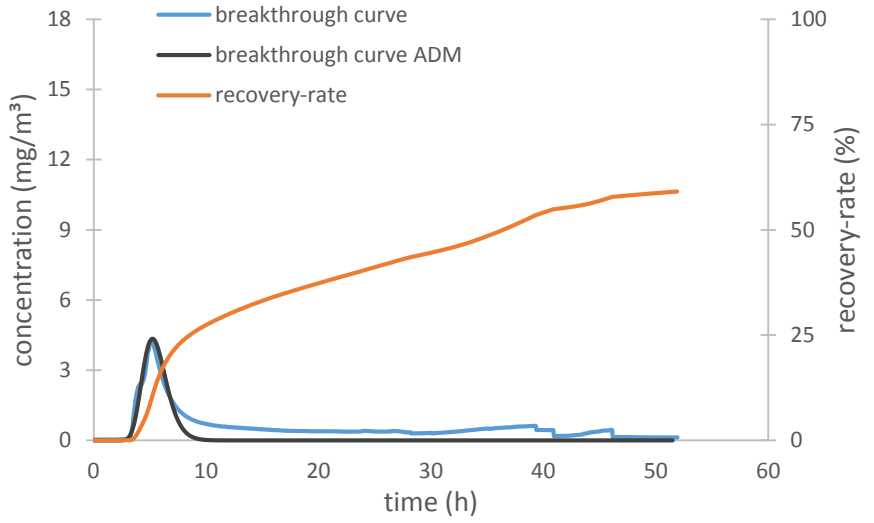

First appearance (h)	3.1
Tracer peak (h)	5.1
50% of total mass (h)	11.6
Amount (corrected) (g)	25
Flow-velocity (m/s)	0.05
Dispersion (m)	20

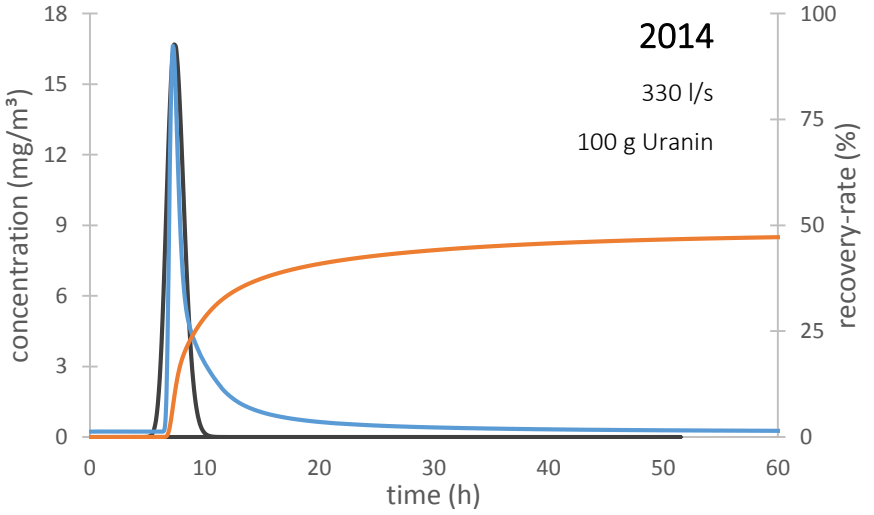

First appearance (h)	6.4
Tracer peak (h)	7.2
50% of total mass (h)	8.9
Amount (corrected) (g)	37
Flow-velocity (m/s)	0.037
Dispersion (m)	5

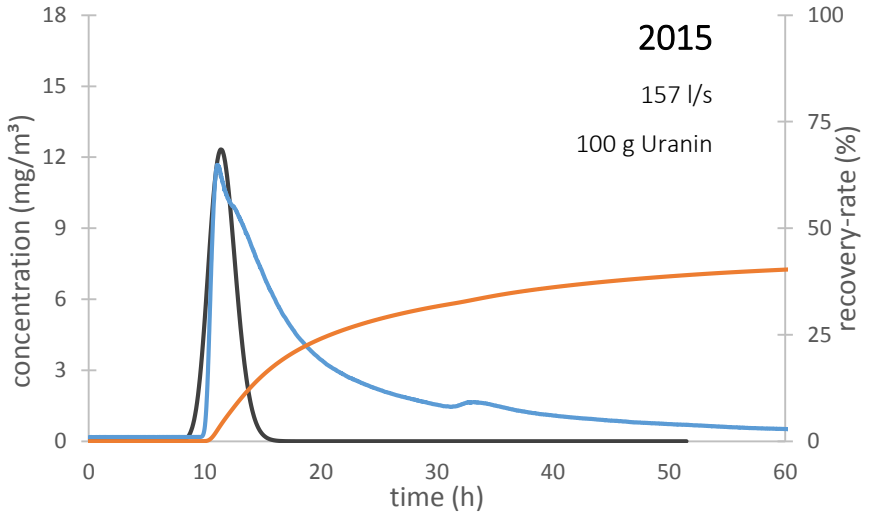

First appearance (h)	9.6
Tracer peak (h)	11.1
50% of total mass (h)	18.7
Amount (corrected) (g)	20
Flow-velocity (m/s)	0.024
Dispersion (m)	5

Figure 4-11: Results of the uranin tracer tests from the years 2013, 2014 and 2015. The fitted advection-dispersion model (ADM) was produced using the formulas by Rausch et al. 2002.

Host rock analysis

The XRD analysis of one of the two host rock samples taken in the field is shown in Figure 4-12. Similar to the second analysis (see Appendix) the host rock south of the EBS is predominantly built up by calcite with minor quartz components. This composition matches the overall composition of the EBS waters which was defined as Ca-HCO_3 / Ca-Mg-HCO_3 dominated. A slight peak-shift within the calcite data suggests the presence of Mg-Calcite, which would coincide with the magnesium enrichment in the water samples.

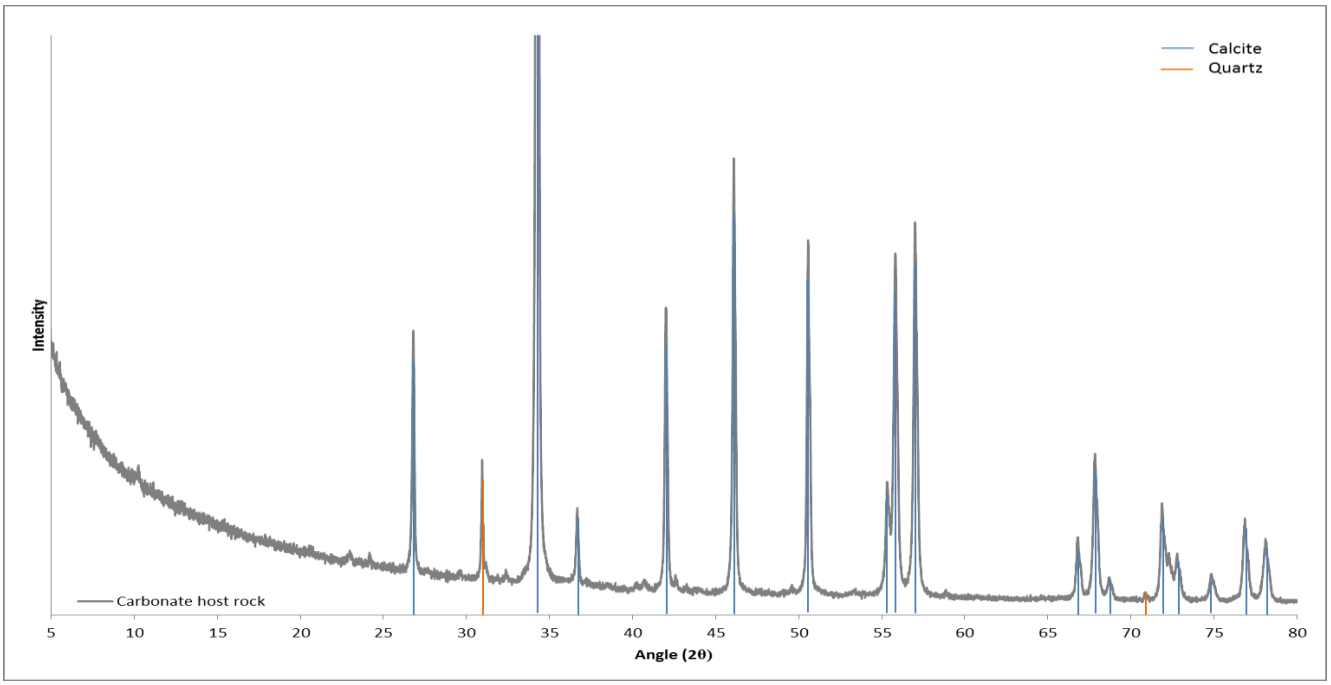

Figure 4-12: XRD-Analysis of the carbonate host rock. The sample was taken at the uranin tracer test location (s. Figure 2-1).

5 | Discussion

Flow situation

The catchment area is dominated by karstified carbonate rocks and the composition of the solution resembles the dissolution of calcite with minor contents of magnesium similar to the host rock samples. However, two groups of waters have been identified. On the one hand waters with an overall stable trend throughout the year and little to no response to high discharge events. They show little variation in discharge volume (s. Table 4-1), temperature and pH, represent the maximum ion concentrations for this data set and are characterized by the heaviest water isotope signal. On the other hand, waters with lighter isotope signatures and a seasonal discharge regime can be described. Their ionic composition correlates inversely with the discharge volume. Shuster and White (1971) discussed the seasonal variations of springs in limestone-dominated areas and found that conduit systems show large variations in concentrations, temperature and discharge over the year, compared to fissure/matrix system springs with an overall stable behavior in respect to the ion concentrations. Their index used for classification was the variance of the hardness (expressed as ppm of dissolved $CaCO_3$ in the water) with fissured system variances < 5 % and conduit systems with variances between 10 – 24 %. In this case, the outlets from the basin and the bulk sample (#2, #3, #4, #5, #6, #7, #9) show a variance range from 10 - 30% compared the lateral outlets (#0, #1, #8) with a value range between 5 – 7 %. Incorporating the previously discussed variations of discharge, concentration and temperature to the variance of hardness, a differentiation between matrix-system dominated waters surfacing at the sides of the spring and conduit-system dominated waters surfacing at the basin of the EBS is indicated.

Furthermore, the findings of Martin and Dean (2001) state that the concentrations generally increase during low flow concentrations because of a greater matrix contribution. Utilizing Figure 5-1 the differentiation between samples from the conduit system and the matrix system is relatively simple. Samples associated with the conduit system show an apparent trend towards the matrix system properties. The closer the samples plot towards the matrix system regime, the lower the overall discharge volume.

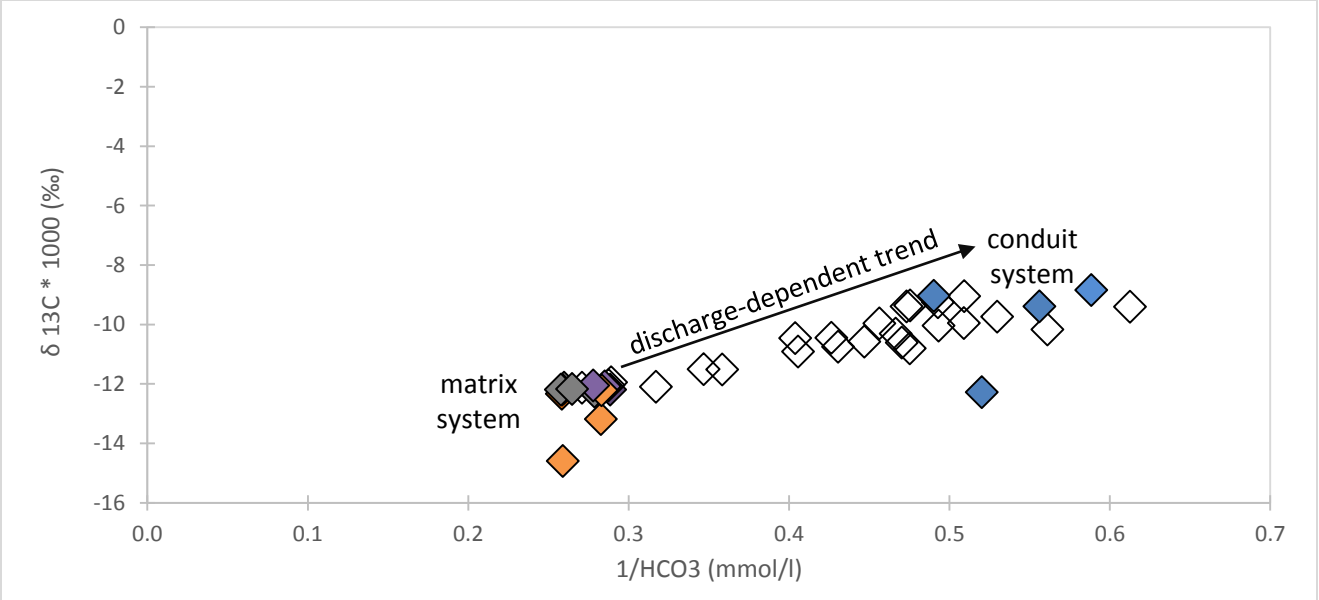

Figure 5-1: Plot of δ δ $^{13}C_{DIC}$ in ‰ relative to VPDB vs. the reverse concentration of HCO_3. Partition in conduit system samples and matrix system samples. Color scheme: #0 (orange), #1 (purple), #2-#7 (white), #8 (dark grey), #9 (blue).

Another aspect characterizing the evolution of the spring waters is their calcite dissolution behavior. Figure 5-2 displays the EBS water samples compared to the evolution of HCO_3 and pH with different initial partial pressures for CO_2 in an open or closed system after Clark and Fritz (1997). Nearly all samples plot along the line for calcite saturation (as already shown in Figure 4-7(a) with the exception of #0 "pool" samples. Additionally, the mean $\delta\ ^{13}C_{DIC}$ value for the matrix system (-12.5 ‰) and conduit system (-10.4 ‰) are added. The #0 "pool" samples trace an evolution based on closed system conditions usually encountered within carbonate rock terrains without ongoing gaseous CO_2 exchange and a dominant C_3 vegetation cover. Infiltrating precipitation absorbs CO_2 from the present vegetation cover and is thus capable of carbonate host rock dissolution. The $\delta\ ^{13}C_{DIC}$ value for waters originating in a closed system with C_3 vegetation cover and an initial pCO_2 of around $10^{-1.5}$ atm have an isotopically lighter initial $\delta\ ^{13}C_{DIC}$ value of -12.5 ‰. Matrix system waters therefore originate from an area with a thick vegetation cover that results in a strongly increased initial pCO_2 value of the water transiting from the soil to the vadose zone.

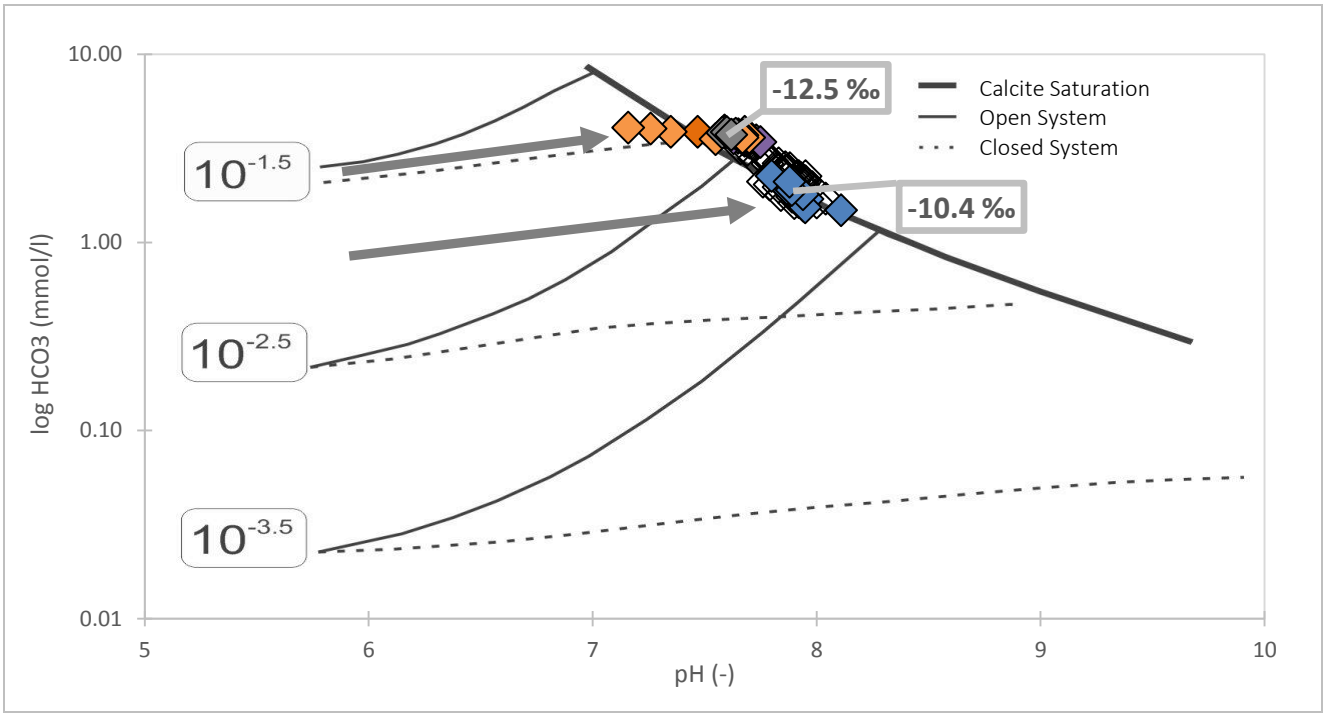

Figure 5-2:Plot of the EBS-water samples within the calcite dissolution system starting from different pCO_2 values on the right. The values above the samples represent the mean $\delta\ ^{13}C_{DIC}$ value for the fissured and conduit system respectively. Edited after Clark and Fritz (1997). Color scheme: #0 (orange), #1 (purple), #2-#7 (white), #8 (dark grey), #9 (blue).

Following a closed system evolution similar to the matrix system samples an initial pCO_2 of $10^{-2.0}$ can be assumed for the conduit system, too. The resulting $\delta\ ^{13}C_{DIC}$ value should be around -12.4 to -12.3 ‰ (e.g. Clark and Fritz (1997). The actual value of -10.4 ‰ could be explained with an initially higher $\delta\ ^{13}C_{DIC}$ value due to C_4 vegetation, but the fraction of C_4 vegetation, especially in altitudes above 1000 m, is negligible (Still et al 2003). Another reason for elevated initial $\delta\ ^{13}C_{DIC}$ values is the fractionation caused by superficial water flow and the associated CO_2 degassing. Doctor et al (2008), Ali & Atekwana (2009) and Abongwa & Atekwana (2013) investigated the evolution of stable carbon isotopes in surface waters with flow time and were able to establish a relationship between surface water flow time and $\delta\ ^{13}C_{DIC}$ value. An increase of 3 – 5 ‰ in $\delta\ ^{13}C_{DIC}$ values was observed by Doctor et al (2008) within a distance of 0.5 km, concomitant with increasing pH and decreasing pCO_2.

Waters originating in the Bärenkar travel approximately 1 km from the center of the Bärenkar to the tracer input location. During this time the stream water has enough time for CO_2 exchange with the atmosphere, increasing its $\delta\ ^{13}C_{DIC}$ value significantly. After passing by the uranin input location the creek water infiltrates into the karst system, where it follows the same closed system evolution as the matrix system waters with the difference of an initially increased $\delta\ ^{13}C_{DIC}$ values. Waters from the conduit system surfacing at the EBS therefore display a 2.1 ‰ increased $\delta\ ^{13}C_{DIC}$ value.

Groundwater mixing

As discussed in the previous chapter waters of the ESB can be divided into a type dominated by the matrix system, one dominated by the conduit system and some samples with alternating properties somewhere in between those two groups. Normally, springs are described as temporally either matrix or conduit system dominated, the influence of a matrix system component during low flow conditions is also found for conduit system dominated springs (Martin and Dean, 2001). In this case both types of waters originate at different outlets at the same geographical location at the same time. As their chemical and isotopic properties are known, it is therefore possible to calculate the mixing fractions. The application of a mixing calculation requires the definition of two end-members. Varying sampling locations and the iron excess discard #0 as possible end member. #9, as a bulk sample, is already influenced by both water types and therefore not suited as end-member. The outlets #1 and #8 are quite similar in their chemical and isotopic characteristics but as the mixing process seems to happen primarily at the outlets #2 and #3, and #8 is not related to those locations. Outlet #1 will therefore serve as the endmember for the matrix water type. The end-member for the conduit system is represented by waters furthest away from #1 but still located in the basin, making #7 the most suitable location. Clark 2015 offers a calculation using the stable carbon isotope signal in combination with its solute HCO_3. As the isotope of a solute being dependent on the solute concentration itself, the mixing trend follows a curve, not a straight line. The Equation

$$f_{fiss} = \frac{\delta^{13}C_{out} * m(HCO_3)_{out} - \delta^{13}C_{cond} * m(HCO_3)_{cond}}{\delta^{13}C_{fiss} * m(HCO_3)_{fiss} - \delta^{13}C_{cond} * m(HCO_3)_{cond}}$$

takes the concentration-dependence into consideration. With f_{fiss} representing the fraction of matrix water contributing to the sample. The notation “out” stands for the outlet calculated, “fiss” for fissured (matrix) system component and “cond” for conduit system component. Consequently, the fraction of conduit system water can be expressed as 1 - f_{fiss}. With the help of this equation the fractions contributing to the respective outlets can be calculated for each fieldtrip. Figure 5-3 summarizes the results for the fieldtrips 1, 2, 4 and 7 (these fieldtrips featured carbon isotope sampling) with the correlation for $\delta\ ^{13}C_{DIC}$ and the reverse concentration of HCO_3 on the left side and the resulting water composition on the right side of the figure including the corresponding discharge value. During low discharge conditions (51 l/s) the matrix system contributes strongly to the sampling locations on the left side of the basin (#2, #3, #4) with decreasing influence towards the right side. With intermediate discharge the dominance of the matrix system is reduced, only outlet #3 is significantly influence by the matrix system water. A high discharge volume (372 l/s) suppresses the influence of matrix system water below 30 % in all outlets.

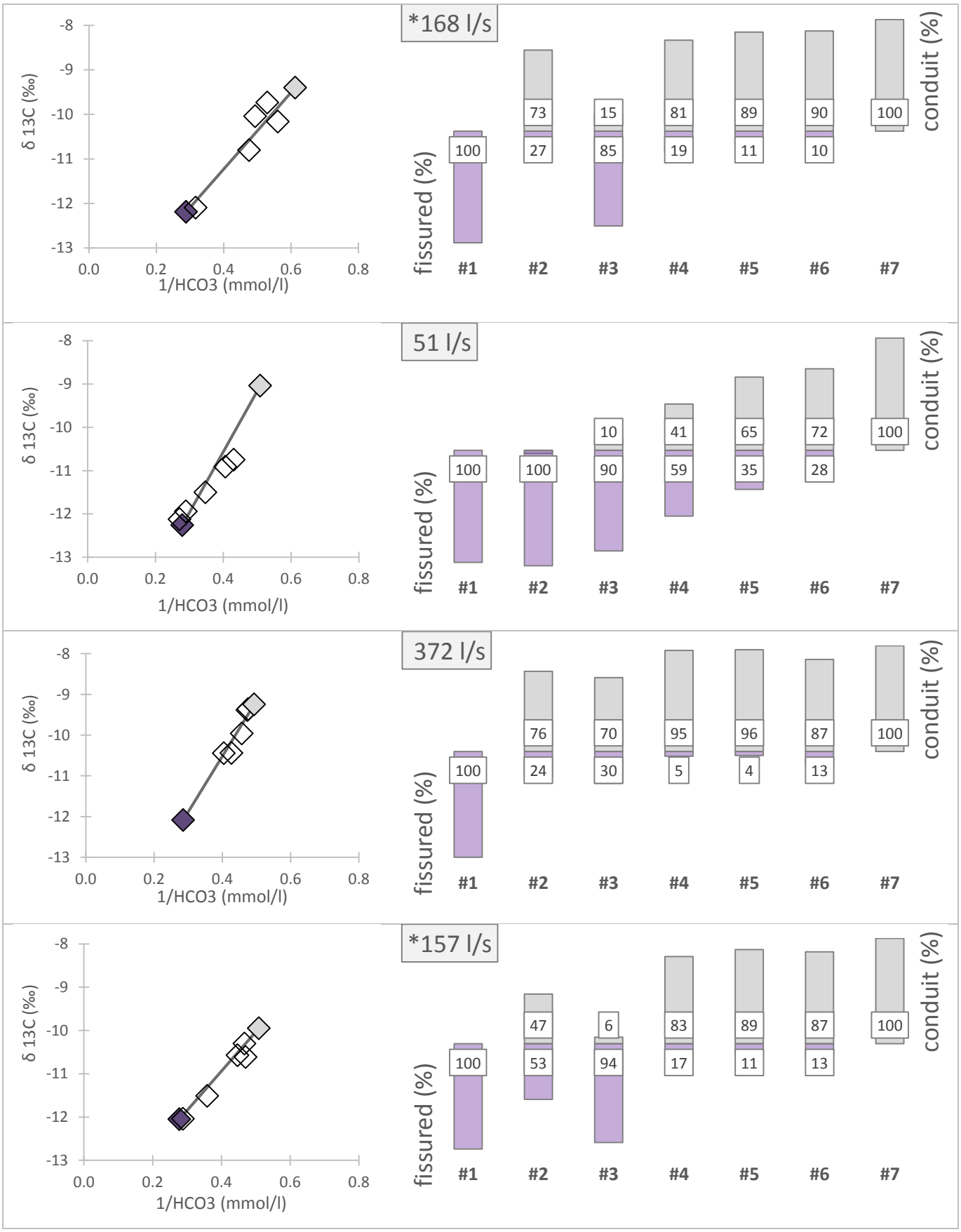

*Figure 5-3: (LEFT) Plot of δ $^{13}C_{DIC}$ in ‰ relative to VPDB vs. the reverse concentration of HCO_3 and (RIGHT) the fractions (matrix/conduit system water) contributing to the total composition of the outlets. Endmembers used for calculation were #1 (purple) for the matrix system and #7 (grey) for the conduit system. *This discharge value was measured further downstream and does not represent the actual spring discharge but yields an order of magnitude for the comparison with the other fieldtrips.*

As Figure 5-3 shows an evident influence of fissured/matrix system water this influence should also be present at the bulk sample #9. Figure 5-4 compares the signatures of the endmembers #1 and #7 with the signal from #9 and shows clearly, that the bulk samples plot within the same area as #7. The addition of water with the characteristics of #1 would be expected to plot somewhere in between (blue circle). To the contrary, the bulk samples show a rather opposing trend with similar or even higher $\delta\ ^{13}C_{DIC}$ values than the assumed "endmember" #7.

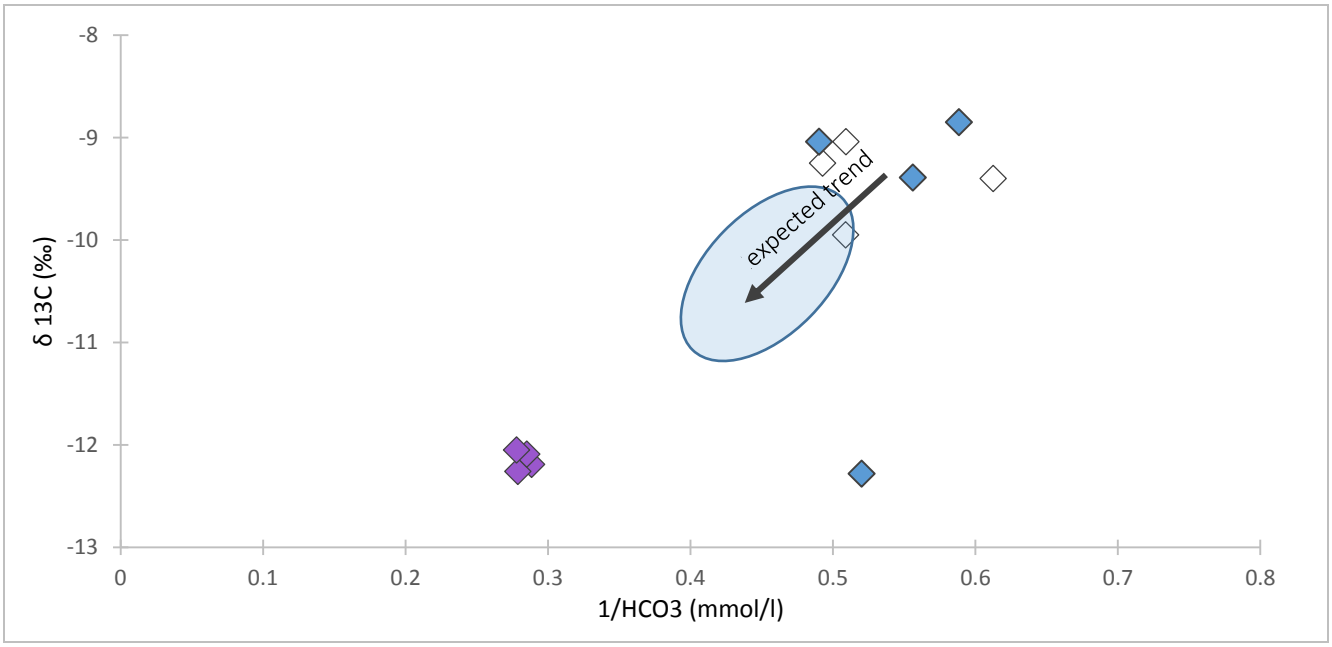

Figure 5-4: Comparison between the endmembers for the mixing calculation #1 (purple) and #7 (white) and the bulk sample from #9 (blue).

Thus, the influence of matrix system water can only be established for sampling locations at the rim of the EBS, whereas the overall composition of the EBS is determined by conduit-system water. Matrix-system water is admittedly present, but is subordinate to the bulk water chemistry.

Altitude difference

As already mentioned while describing the oxygen isotope data, an altitude difference of 684 m within the samples could be calculated assuming a fractionation of -0.19 ‰ per 100 m. Incorporating the findings of the carbon isotopes and the groundwater mixing process a more precise calculation can be performed. Therefore, the maximum altitude difference will be calculated using the $\delta\ ^{18}O$ values of the endmembers used in the mixing calculation. The outlets #1 and #7 represent the matrix system and conduit system flow respectively.

Table 5-1 shows the results of this calculation and in addition the respective predominant discharge volume of the EBS. Altitude difference between 32 and 526 meters have been calculated with the highest differences correlating with the highest discharge. Although no absolute elevations information can be given, it appears that different outlets of EBS recharge in different catchment areas. Whereas low discharge is related to a comparably homogeneous elevation, high discharge includes areas of higher elevations. Transferring these findings onto the study area and including the findings of the carbon isotopes suggest that the catchment area accountable for the low flow regime seems to be autogenic. It is represented by the formations of the ore-bearing carbonate rocks itself, extending from the EBS (855 m asl) to the summit

of the Grieskogel (1495 m asl). High discharge conditions are primarily fed by an allogenic recharge from the "upper" catchment areas e.g. such as the Bärenkar ranging from 1255 m (tracer input) up to 1782 m (Rotkogel). The medians of these two catchment areas are 1175 m and 1520 m respectively, resulting in a median difference of 344 m, which fits pretty well to the isotopic signature differences.

Table 5-1: Calculation of the altitude difference between samples from outlet #1 and outlet #7 using a fractionation of -0.19 ‰ per 100 m for each fieldtrip featuring oxygen isotope sampling.

$\delta^{18}O$ (‰)	10.3.15	14.4.15	10.5.15	19.5.15	8.6.15	12.7.15
#1	-11.22	-11.51	-11.32	-11.59	-11.52	-11.57
#7	-11.37	-12.11	-12.32	-12.13	-11.93	-11.63
#1 - #7	0.15	0.60	1.00	0.54	0.41	0.06
Altitude difference (m)	**79**	**316**	**526**	**284**	**216**	**32**
Discharge (l/s)	75	412	443	277	157	109

Unique characteristic of outlet #0

An interesting unique feature of the presented data are the outliers from #0 taken in the original pool. These samples are characterized by significantly lower pH-values and sulfate concentrations, high iron concentrations but an overall similar chemistry compared to the samples from the margins of the EBS. This similarity suggests a matrix system origin but with an average concentration of 10.4 mg/l the water in the pool is highly oversaturated with iron oxides/-hydroxides.

As already mentioned in the description of the study site, ore-mining was common within the formations of the ore-bearing carbonate rock units and still exists at the Erzberg about 20 km east of our study area. Based on the idea of different flow channels within the karstified aquifer, it is quite possible that one of these many flow channels is associated with an ore bearing lens. The dissolution of Siderite and/or Ankerite is a probable cause for increasing iron concentrations but it does not affect the overall water chemistry significantly. Whereas the groundwater contains less oxygen during its time in the aquifer making it possible to take up high amounts of ionic iron, the oxygen content increases dramatically when the water surfaces and is exposed to the atmosphere. As supersaturation in respect to iron is reached, precipitation of iron oxide/hydroxides, mostly Goethite (FeO(OH)) starts (Hem 1962). Precipitation of iron-hydroxides can explain the brownish/reddish color of the water surfacing in the #0 "pool".

6 | Conclusion

Summary

Varying field parameters at the Etzbach Spring are caused by the mixture of two different types of waters.
Predominant during low flow conditions are the waters originating from the autogenic system of the carbonate rocks within the catchment area. These waters are characterized by the following properties:

- Higher Temperature and EC, lower pH
- Constant discharge
- High mineralization
- Slightly oversaturated with calcite
- Heavier $^{18}O/D$ values -> origin in lower altitudes
- Lighter $^{13}C_{DIC}$ signature -> origin from an area with soil cover and higher CO_2 partial pressure

On the contrary are the waters originating from the allogenic system transported several hundreds of meters per hour through conduits of the karst system. These waters are dominant during high discharge conditions and are partially fed by allogenic precipitation, e.g. from the Bärenkar. Their characteristics are:

- Lower Temperature and EC, higher pH
- Strongly variable discharge
- Lower mineralization
- Slightly undersaturated with calcite
- Lighter $^{18}O/D$ values -> origin in higher altitudes
- Heavier $^{13}C_{DIC}$ signature -> superficial flow as part of the Bärenkar Creek before infiltration into carbonate rocks

Figure 6-1 shows a conceptual model for the flow situation at the EBS with the two respective water types. Whereas the matrix-system water surfaces at the margin of the spring in the area of #0 and #1, conduit spring water becomes more dominant in the central depression (basin) area towards #7. The increasing dominance towards the basin may be explainable with the concept of an overflow spring situation for the conduit-system water. As mentioned, the surroundings of the EBS contain a vast swampy area with a shallow groundwater level. The origin of the swampy area may be traced back to the fact that the upper JBT was damned after glaciation and the sedimentation of fine-grained material produced a comparably low conductive barrier. The results are a shallow groundwater level above said barrier and the overflow of the deeper infiltrated groundwater at the edge of the barrier, which is in this case the EBS.
Furthermore, the discrepancy between the total discharge and the estimated runoff (Table 4-1) can also be explained. Even with little runoff, only 20 % of the total volume is affiliated with the sampling locations, leaving the majority of runoff volume to the central region of the basin. Consequently 80% of the total volume (for low discharge conditions) is delivered by the central basin. These 80 % have to be conduit-system water, otherwise the bulk chemistry at location #9 would show a strong matrix-system influence (s. Figure 5-4).

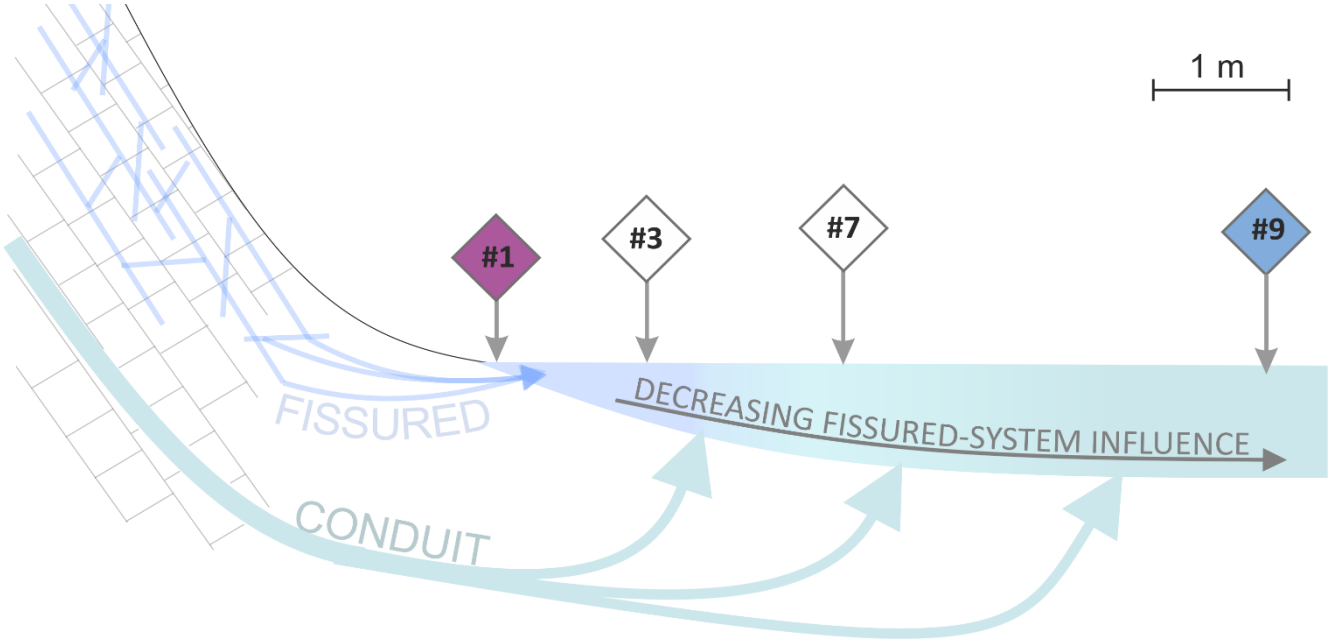

Figure 6-1: Schematic illustration of the flow situation at the EBS. The figure shows a theoretical cross section through the EBS from S to N. Note that the displayed sampling locations are ordered by degree of fissured/matrix-system influence and not by their actual geographical location.

Outlook

Some questions still remain open or deserve more intense study. First of all, an investigation concerning the structure and sedimentary build-up of the upper JBT valley filling, especially in the area around the EBS would be important. This information could give an answer to the assumption of an overflow spring being correct.

Additional sampling locations could be favorable to asses some specifics of the system, such as a deep-probing of the spring basin, giving information about the upwelling basin water. Furthermore, the upwelling water on the forest road below #0 and #1 should be sampled and compared with the existing data.

To assess the relationship between the spring discharge and the runoff of the Bärenkar Creek (BKC), additional discharge measurements at the BKC above the sinking should be conducted. Furthermore, research regarding the discharge balance is needed. The discharge of the BKC and the topographical catchment area from Figure 2-1 is not nearly enough to achieve the water volumes discharged by the EBS. That is why the actual recharge area is probably even larger than the Bärenkar itself and further tracer tests in more remote locations could be suitable.

The chemical composition of the #0 “pool” deserves a more extensive investigation, regarding the structure of the precipitates, the origin of the iron content and the evolution within the aquifer.

As a matter of fact, the Odlstein cave possesses an internal spring that re-filtrates into the carbonate rocks. Chemical analysis of this water could offer information about the aquifer-internal evolution of the water and the spring could be used to conduct an uranin tracer test to confirm a connection between the Odlstein cave and the EBS.

7 | References

Abongwa, P. T. & Atekwana, E. A. (2013). Assessing the temporal evolution of dissolved inorganic carbon in waters exposed to atmospheric CO2(g): A laboratory approach. *Journal of Hydrology*. Elsevier B.V. **505**, 250–265.

Ali, H. N. & Atekwana, E. A. (2009). Effect of progressive acidification on stable carbon isotopes of dissolved inorganic carbon in surface waters. *Chemical Geology*. Elsevier B.V. **260**, 102–111.

Atkinson, T. C. (1977). Diffuse flow and conduit flow in limestone terrain in the Mendip Hills, Somerset (Great Britain). *Journal of Hydrology* **35**, 93–110.

Basemap.at (2016). Website for administrative base maps in Austria. http://www.basemap.at/ Accessed in Juli 2016.

Clark, I. (2015). Groundwater Geochemistry and Isotopes. 456 pp., CRC Press/Lewis Publishers, Boca Raton, FL.

Clark, I. D. & Fritz, P. (1997). Environmental isotopes in hydrogeology. 328 pp., CRC Press/Lewis Publishers, Boca Raton, FL.

Doctor, D. H., Kendall, C., Sebestyen, Stephen, D., Shanley, James, B., Ohte, N. & Boyer, Elizabeth, W. (2008). Carbon isotope fractionation of dissolved inorganic carbon (DIC) due to outgassing of carbon dioxide from a headwater stream. *Hydrogeological Processes* **22**, 2267–2274.

Hager, B. & Foelsche, U. (2015). Stable isotope composition of precipitation in Austria. *Austrian Journal of Earth Sciences* **108/2**, 2–13.

Hem, J. D. (1962). Chemistry of iron in natural water. *U.S. G.P.O.,Water Supply Paper 1459-I, iv, 268 p.*

Hießleitner, G. (1935). Zur Geologie der Erz führenden Grauwackenzone des Johnsbachtales. *Jahrbuch der Geologischen Bundesanstalt* **85**, 81–100.

Hießleitner, G. (1958). Zur Geologie der Erz führenden Grauwackenzone zwischen Admont-Selzthal-Liezen. *Jahrbuch der Geologischen Bundesanstalt* **99**, 35-77.

Jacobson, R. L. & Langmuir, D. (1974). Controls on the quality variations of some carbonate spring waters. *Journal of Hydrology* **23**, 247–265.

JAWAD, S. B. & HUSSIEN, K. A. (1986). Contribution to the study of temporal variations in the chemistry of spring water in karstified carbonate rocks The temporal variations of spring water. *Hydrological Sciences Journal* **31**, 529–541.

LaMoreaux, P. E. (2001). *Springs and Bottled Waters of the World*. Springer-Verlag Berlin Heidelberg New York Library.

Lieb, G. K. & Premm, M. (2008). Werdegang und Dynamik im Formenbild eines zweigeteilten Tales. *Schriften des Nationalparks Gesäuse*, 12–24.

Mandl, G. W. (2000). The Alpine sector of the Tethyan shelf - Examples of Triassic to Jurassic sedimentation and deformation from the Northern Calcareous Alps. *Mitt. Österr. Geol. Ges.* **92**, 61–77.

Martin, J. B. & Dean, R. W. (2001). Exchange of water between conduits and matrix in the Floridan aquifer. *Chemical Geology* **179**, 145–165.

Probst, G. (1993). Erfassung der Wasserreserven in den Eisenerzer Alpen (Steiermark). *Arch. f. Lagerst.forsch. Geol.B.-A.* **14**, 109–117.

Rausch, R., Schäfer, W., & Wagner, C. (2002). Einführung in die Transportmodellierung im Grundwasser. 183 pp., Borntraeger, Berlin/Stuttgart.

Redlich, K. A. (1920). Das Johnsbachtal. *Austrian Journal of Earth Sciences* **15**, 305–312.

Redlich, K. A. (1922). Der Erzzug Vordernberg - Johnsbachtal. *Austrian Journal of Earth Sciences* **15**, 207–262.

Révész, K. M., & Landwehr J. M. (2002). Delta13C and delta18O isotopic composition of CaCO3 measured by continuous flow isotope ratio mass spectrometry: statistical evaluation and verification by application to Devils Hole core DH-11 calcite. *Rapid Commun Mass Spectrom* **16**(22) 2-14.

Schnegg, P. (2003). A new field fluorometer for multi-tracer tests and turbidity measurement applied to hydrogeological problems. *8th IInternational Congress of the Brazilian Geophysical Society held in Rio de Janeiro, Brazil*, 8–10.

Schönlaub, H. P. (1982). Die Grauwackenzone in den Eisenerzer Alpen (Österreich). *Jahrbuch der Geologischen Bundesanstalt* **124**, 361–423.

Schönlaub, H. P., Flajs, G. & Thalmann, F. (1980). Conodontenstratigraphie am Steirischen Erzberg (Nördliche Grauwackenzone). *Jahrbuch der Geologischen Bundesanstalt* **123**, 169–229.

Shuster, E. T. & White, W. B. (1971). Seasonal fluctuations in the chemistry of lime-stone springs: A possible means for characterizing carbonate aquifers. *Journal of Hydrology* **14**, 93–128.

Simunek, J., Van Genuchten, M. T., Sejna, M., Toride, N. & Leij, F. (1999). The STANMOD computer software for evaluating solute transport in porous media using analytical solutions of convection–dispersion equation. Versions 1.0 and 2.0. *Golden (CO)*.

Spötl, C., & Vennemann, T. W. (2003). Continuous-flow isotope ratio mass spectrometric analysis of carbonate minerals. *Rapid communications in mass spectrometry* **17**(9), 1004-1006.

Still, C. J., Berry, J. A., Collatz, G. J. & DeFries, R. S. (2003). Global distribution of C 3 and C 4 vegetation: Carbon cycle implications. *Global Biogeochemical Cycles* **17**, 6–1–6–14.

Strasser, U., Marke, T., Sass, O., Birk, S. & Winkler, G. (2013). John's creek valley: A mountainous catchment for long-term interdisciplinary human-environment system research in Upper Styria (Austria). *Environmental Earth Sciences* **69**, 695–705.

UBA (2016). Website of the Environment Agency Austria. http://www.umweltbundesamt.at/ Accessed in April 2016.

WegenerNet (2015). Website of the data portal "Gesäuse" from the Wegener Center Graz. http://www.bogner-lehner.net/xeis_datenportal_en.php Accessed in December 2015.

Appendix

Table A-1: Field data, water chemistry and isotopes at the given date ordered by outlet number.

10.11.14										
Outlet	#0	#1	#2	#3	#4	#5	#6	#7	#8	#9
Field data										
Electric cond. (µS/cm)	379	342	223	320	197	176	206	177	372	173
Temperature (°C)	7.3	7.1	6.5	7	6.4	6.3	6.5	6.4	6.9	6.3
pH-Value (-)	7.47	7.68	7.76	7.66	7.79	7.9	7.84	7.92	7.59	7.96
Oxygen sat. (mg/l)	0.25	7.97	9.83	8.9	10.59	10.71	10.62	10.79	7.49	10.75
Water-Chemistry (mmol/l)										
HCO3 (mmol/l)	3.8689	3.4646	2.1042	3.1554	2.0273	1.8882	1.7821	1.6325	3.8473	1.6992
F (mmol/l)	0.0011	0.0016	0.0014	0.0015	0.0011	0.0008	0.0007	0.0009	0.0014	0.0010
Cl (mmol/l)	0.1381	0.0515	0.0176	0.0434	0.0133	0.0094	0.0086	0.0066	0.0431	0.0077
NO3 (mmol/l)	0.0034	0.0601	0.0554	0.0634	0.0530	0.0502	0.0486	0.0478	0.0462	0.0498
SO4 (mmol/l)	0.0000	0.1627	0.0506	0.1522	0.0492	0.0391	0.0423	0.0388	0.2331	0.0405
Al (mmol/l)	0.0012	0.0009	0.0009	0.0011	0.0007	0.0006	0.0005	0.0005	0.0009	0.0003
Ba (mmol/l)	0.0005	0.0002	0.0002	0.0002	0.0002	0.0002	0.0002	0.0002	0.0003	0.0002
Ca (mmol/l)	1.5916	1.5796	0.9932	1.4692	0.9237	0.8419	0.8155	0.7718	1.6690	0.7823
Fe (mmol/l)	0.1150	0.0005	0.0004	0.0001	0.0001	0.0001	0.0001	0.0001	0.0000	0.0001
K (mmol/l)	0.1006	0.0177	0.0105	0.0156	0.0106	0.0085	0.0086	0.0079	0.0193	0.0083
Li (mmol/l)	0.0002	0.0003	0.0002	0.0003	0.0002	0.0001	0.0001	0.0001	0.0003	0.0001
Mg (mmol/l)	0.2882	0.3396	0.1773	0.2689	0.1636	0.1557	0.1607	0.1577	0.4483	0.1549
Na (mmol/l)	0.0583	0.0839	0.0443	0.0728	0.0389	0.0351	0.0348	0.0331	0.0864	0.0335
P (mmol/l)										
Si (mmol/l)	0.1299	0.1057	0.0851	0.1049	0.0860	0.0841	0.0824	0.0762	0.1008	0.0778
Sr (mmol/l)	0.0017	0.0022	0.0010	0.0018	0.0010	0.0009	0.0009	0.0009	0.0030	0.0009
S (mmol/l)	0.0218	0.1045	0.0551	0.0559	0.0505	0.0464	0.0475	0.0488	0.2567	0.0487
Isotopes										
$\delta^{18}O$ (‰ VSMOW)										
$\delta^{2}H$ (‰ VSMOW)										
$\delta^{13}C$ (‰ VSMOW)	-12.33	-12.19	-10.8	-12.09	-10.04	-9.73	-10.16	-9.4	-12.13	-8.85

Table A-2: Field data, water chemistry and isotopes at the given date ordered by outlet number.

19.12.14										
Outlet	#0	#1	#2	#3	#4	#5	#6	#7	#8	#9
Field data										
Electric cond. (µS/cm)	379	342	346	323	271	235	221	195	365	185
Temperature (°C)	7.2	7	7	7.1	6.8	6.8	6.7	6.5	7	6.5
pH-Value (-)	7.55	7.65	7.64	7.69	7.77	7.82	7.84	7.83	7.68	7.87
Oxygen sat. (mg/l)	5.12	8.13	8.05	8.46	9.5	10.14	10.43	10.46	8.74	10.62
Discharge (%)										
Water-Chemistry (mmol/l)										
HCO3 (mmol/l)	3.5372	3.5862	3.6908	3.4594	2.8849	2.4654	2.3223	1.9642	3.8666	1.9221
F (mmol/l)	0.0014	0.0014	0.0013	0.0013	0.0011	0.0008	0.0008	0.0007	0.0015	0.0007
Cl (mmol/l)	0.0515	0.0484	0.0450	0.0450	0.0332	0.0215	0.0173	0.0107	0.0442	0.0105
NO3 (mmol/l)	0.0679	0.0602	0.0580	0.0672	0.0622	0.0874	0.0635	0.0588	0.0542	0.0510
SO4 (mmol/l)	0.1521	0.1597	0.1718	0.1498	0.0959	0.0674	0.0601	0.0664	0.1956	0.0602
Al (mmol/l)	0.0020	0.0021	0.0020	0.0019	0.0018	0.0016	0.0015	0.0018	0.0021	0.0013
Ba (mmol/l)	0.0003	0.0003	0.0003	0.0003	0.0003	0.0003	0.0003	0.0002	0.0003	0.0002
Ca (mmol/l)	1.6456	1.6660	1.6413	1.4909	1.3110	1.1107	1.0582	0.8602	1.6448	0.8361
Fe (mmol/l)	0.0001	0.0000	0.0000	0.0000	0.0000	0.0000	0.0000	0.0001	0.0000	0.0000
K (mmol/l)	0.0221	0.0241	0.0228	0.0197	0.0163	0.0145	0.0146	0.0128	0.0246	0.0113
Li (mmol/l)	0.0004	0.0004	0.0004	0.0003	0.0003	0.0002	0.0002	0.0002	0.0004	0.0002
Mg (mmol/l)	0.3661	0.3975	0.4009	0.3461	0.2584	0.2083	0.1909	0.2149	0.4770	0.1992
Na (mmol/l)	0.0982	0.1005	0.0958	0.0897	0.0770	0.0666	0.0613	0.0580	0.1029	0.0561
P (mmol/l)	0.0038	0.0032	0.0030	0.0033	0.0026	0.0032	0.0031	0.0030	0.0022	0.0027
Si (mmol/l)	0.0996	0.0975	0.0947	0.0954	0.0923	0.0907	0.0887	0.0816	0.0917	0.0801
Sr (mmol/l)	0.0024	0.0026	0.0027	0.0022	0.0016	0.0012	0.0011	0.0013	0.0031	0.0012
S (mmol/l)	0.1759	0.1814	0.1892	0.1622	0.1152	0.0903	0.0768	0.0833	0.2215	0.0821
Isotopes										
$\delta^{18}O$ (‰ VSMOW)										
$\delta^{2}H$ (‰ VSMOW)										
$\delta^{13}C$ (‰ VSMOW)	-13.18	-12.26	-12.12	-11.94	-11.5	-10.91	-10.75	-9.04	-12.19	-12.28

Table A-3: Field data, water chemistry and isotopes at the given date ordered by outlet number.

24.3.15										
Outlet	#0	#1	#2	#3	#4	#5	#6	#7	#8	#9
Field data										
Electric cond. (µS/cm)	365	371	381	374	315	266	270	234	401	231
Temperature (°C)	7.1	7	6.9	7.1	6.7	6.7	6.7	6.6	7.2	6.7
pH-Value (-)	7.63	7.63	7.65	7.62	7.69	7.78	7.8	7.82	7.59	7.8
Oxygen sat. (mg/l)										
Discharge (%)	30		20		5	10	8	7	20	
Water-Chemistry (mmol/l)										
HCO3 (mmol/l)	3.6174	3.7046	3.7500	3.7028	3.0993	2.6160	2.7048	2.1966	3.9248	2.2486
F (mmol/l)	0.0013	0.0013	0.0013	0.0014	0.0010	0.0008	0.0009	0.0007	0.0015	0.0007
Cl (mmol/l)	0.0410	0.0384	0.0360	0.0372	0.0397	0.0215	0.0209	0.0135	0.0320	0.0153
NO3 (mmol/l)	0.0561	0.0521	0.0484	0.0510	0.0581	0.0579	0.0627	0.0485	0.0433	0.0513
SO4 (mmol/l)	0.1618	0.1753	0.2000	0.1832	0.1124	0.0744	0.0657	0.0796	0.2483	0.0742
Al (mmol/l)	0.0021	0.0020	0.0022	0.0020	0.0018	0.0017	0.0018	0.0014	0.0022	0.0016
Ba (mmol/l)	0.0003	0.0003	0.0003	0.0003	0.0003	0.0003	0.0003	0.0003	0.0003	0.0003
Ca (mmol/l)	1.7690	1.6743	1.7399	1.7458	1.4868	1.2498	1.2893	0.9801	1.8423	1.0502
Fe (mmol/l)	0.0000	0.0000	0.0000	0.0000	0.0000	0.0000	0.0000	0.0000	0.0000	0.0000
K (mmol/l)	0.0232	0.0221	0.0246	0.0245	0.0180	0.0155	0.0138	0.0105	0.0244	0.0146
Li (mmol/l)	0.0004	0.0004	0.0004	0.0004	0.0003	0.0003	0.0003	0.0002	0.0004	0.0002
Mg (mmol/l)	0.4076	0.4149	0.4464	0.4256	0.3039	0.2410	0.2125	0.2517	0.5080	0.2591
Na (mmol/l)	0.1040	0.0971	0.0973	0.0978	0.0827	0.0685	0.0644	0.0567	0.0935	0.0638
P (mmol/l)	0.0026	0.0027	0.0031	0.0033	0.0031	0.0030	0.0031	0.0035	0.0032	0.0043
Si (mmol/l)	0.1010	0.0966	0.0932	0.0963	0.0943	0.0895	0.0928	0.0811	0.0960	0.0842
Sr (mmol/l)	0.0026	0.0026	0.0028	0.0026	0.0018	0.0013	0.0012	0.0013	0.0033	0.0013
S (mmol/l)	0.1081	0.1123	0.1312	0.1295	0.0862	0.0650	0.0590	0.0620	0.1875	0.0684
Isotopes										
$\delta^{18}O$ (‰ VSMOW)	-11.16	-11.22	-11.21	-11.44	-11.38	-11.35	-11.36	-11.37	-11.67	-11.44
$\delta^{2}H$ (‰ VSMOW)	-79.17	-78.7	-79.6	-80.2	-80.6	-79.5	-79.5	-78.8	-80.9	-79.6
$\delta^{13}C$ (‰ VSMOW)	-13.18	-12.26	-12.12	-11.94	-11.5	-10.91	-10.75	-9.04	-12.19	-12.28

Table A-4: Field data, water chemistry and isotopes at the given date ordered by outlet number.

16.4.15										
Outlet	#0	#1	#2	#3	#4	#5	#6	#7	#8	#9
Field data										
Electric cond. (µS/cm)	378	347	226	233	213	211	217	203	404	204
Temperature (°C)	6.3	7.2	6.3	6.5	6.2	6.2	6.3	6.1	7.4	6.1
pH-Value (-)	7.35	7.69	7.85	7.88	7.9	7.88	7.93	7.94	7.59	7.9
Oxygen sat. (mg/l)										
Discharge (%)	6.7		16.7		13.3	16.7	20.0	23.3	3.3	
Water-Chemistry (mmol/l)										
HCO3 (mmol/l)	3.8602	3.5077	2.3457	2.4769	2.1132	2.1034	2.1915	2.0291	3.8799	2.0396
F (mmol/l)										
Cl (mmol/l)	0.0472	0.0642	0.0226	0.0226	0.0146	0.0137	0.0176	0.0130	0.0422	0.0125
NO3 (mmol/l)		0.0629	0.0755	0.0780	0.0765	0.0757	0.0699	0.0755	0.0476	0.0750
SO4 (mmol/l)	0.0062	0.1180	0.0523	0.0520	0.0397	0.0385	0.0383	0.0419	0.2783	0.0391
Al (mmol/l)	0.0021	0.0020	0.0017	0.0016	0.0014	0.0014	0.0014	0.0013	0.0021	0.0013
Ba (mmol/l)	0.0006	0.0002	0.0002	0.0002	0.0002	0.0002	0.0002	0.0002	0.0003	0.0002
Ca (mmol/l)	1.7335	1.5748	1.1046	1.1435	0.9603	0.9742	1.0919	0.9682	1.8314	0.8923
Fe (mmol/l)	0.2243	0.0000	0.0000	0.0000	0.0000	0.0000	0.0000	0.0000	0.0000	0.0000
K (mmol/l)	0.0196	0.0214	0.0123	0.0129	0.0094	0.0077	0.0104	0.0080	0.0249	0.0086
Li (mmol/l)	0.0001	0.0003	0.0002	0.0002	0.0001	0.0001	0.0001	0.0001	0.0004	0.0001
Mg (mmol/l)	0.2581	0.3405	0.2168	0.2006	0.1704	0.1698	0.1723	0.1841	0.5069	0.1661
Na (mmol/l)	0.0474	0.0935	0.0436	0.0442	0.0280	0.0266	0.0329	0.0266	0.0885	0.0236
P (mmol/l)	0.0025	0.0029	0.0028	0.0032	0.0031	0.0033	0.0033	0.0034	0.0033	0.0036
Si (mmol/l)	0.1159	0.0995	0.0695	0.0736	0.0620	0.0607	0.0657	0.0591	0.0962	0.0577
Sr (mmol/l)	0.0015	0.0022	0.0011	0.0011	0.0008	0.0008	0.0008	0.0009	0.0033	0.0008
S (mmol/l)	0.0218	0.1045	0.0551	0.0559	0.0505	0.0464	0.0475	0.0488	0.2567	0.0487
Isotopes										
$\delta^{18}O$ (‰ VSMOW)	-11.06	-11.51	-11.91	-11.75	-11.86	-11.98	-11.89	-12.11	-11.58	-12.09
$\delta^{2}H$ (‰ VSMOW)	-79.08	-81.4	-83.9	-83.1	-84.8	-84.6	-83.6	-84.7	-82.3	-84.8
$\delta^{13}C$ (‰ VSMOW)	-14.6	-12.09	-10.44	-10.45	-9.39	-9.36	-9.96	-9.25	-12.19	-9.04

Table A-5: Field data, water chemistry and isotopes at the given date ordered by outlet number.

10.5.15										
Outlet	#0	#1	#2	#3	#4	#5	#6	#7	#8	#9
Field data										
Electric cond. (µS/cm)	359	330	164	171	154	154	184	155	392	151
Temperature (°C)	7.3	7.2	5.8	5.8	5.7	5.6	6	5.8	7.4	5.7
pH-Value (-)	7.26	7.75	7.91	7.92	7.94	7.94	7.87	7.9	7.58	8.11
Oxygen sat. (mg/l)										
Discharge (%)	7.1		21.4		19.0	23.8	14.3	9.5	4.8	
Water-Chemistry (mmol/l)										
HCO3 (mmol/l)	4.0254	3.4037	1.7254	1.6866	1.5851	1.5665	1.9206	1.6176	3.8155	1.4796
F (mmol/l)										
Cl (mmol/l)	0.0396	0.0346	0.0094	0.0092	0.0080	0.0069	0.0115	0.0090	0.0522	0.0065
NO3 (mmol/l)	0.0053	0.0609	0.0632	0.0646	0.0633	0.0631	0.0677	0.0607	0.0478	0.0611
SO4 (mmol/l)	0.0012	0.1170	0.0374	0.0356	0.0330	0.0332	0.0386	0.0436	0.2683	0.0320
Al (mmol/l)	0.0022	0.0019	0.0012	0.0011	0.0011	0.0011	0.0014	0.0012	0.0021	0.0011
Ba (mmol/l)	0.0006	0.0002	0.0002	0.0002	0.0002	0.0002	0.0002	0.0002	0.0003	0.0002
Ca (mmol/l)	1.7418	1.5435	0.7828	0.7637	0.6900	0.6879	0.8552	0.6905	1.8013	0.6579
Fe (mmol/l)	0.2689	0.0001	0.0000	0.0000	0.0000	0.0000	0.0000	0.0001	0.0000	0.0000
K (mmol/l)	0.0198	0.0208	0.0095	0.0097	0.0070	0.0088	0.0086	0.0089	0.0249	0.0074
Li (mmol/l)	0.0002	0.0003	0.0001	0.0001	0.0001	0.0001	0.0001	0.0001	0.0004	0.0001
Mg (mmol/l)	0.2984	0.3186	0.1452	0.1407	0.1315	0.1333	0.1383	0.1431	0.4921	0.1318
Na (mmol/l)	0.0567	0.0841	0.0314	0.0310	0.0260	0.0275	0.0324	0.0273	0.0811	0.0252
P (mmol/l)	0.0031	0.0029	0.0025	0.0023	0.0025	0.0026	0.0024	0.0025	0.0023	0.0024
Si (mmol/l)	0.1300	0.0968	0.0676	0.0672	0.0644	0.0644	0.0731	0.0638	0.0961	0.0617
Sr (mmol/l)	0.0017	0.0021	0.0008	0.0008	0.0007	0.0007	0.0008	0.0008	0.0031	0.0007
S (mmol/l)	0.0228	0.1213	0.0465	0.0433	0.0423	0.0409	0.0506	0.0519	0.2803	0.0400
Isotopes										
$\delta^{18}O$ (‰ VSMOW)	-11.45	-11.32	-12.05	-12.22	-12.16	-12.25	-11.91	-12.32	-11.64	-12.36
$\delta^{2}H$ (‰ VSMOW)	-79.81	-79.4	-83.7	-83.9	-83.8	-84.7	-83.1	-84.0	-80.0	-83.6
$\delta^{13}C$ (‰ VSMOW)										

Table A-6: Field data, water chemistry and isotopes at the given date ordered by outlet number.

19.5.15										
Outlet	#0	#1	#2	#3	#4	#5	#6	#7	#8	#9
Field data										
Electric cond. (µS/cm)	359	330	164	171	154	154	184	155	392	151
Temperature (°C)	7.3	7.2	5.8	5.8	5.7	5.6	6	5.8	7.4	5.7
pH-Value (-)	7.26	7.75	7.91	7.92	7.94	7.94	7.87	7.9	7.58	8.11
Oxygen sat. (mg/l)										
Discharge (%)	7.1		21.4		19.0	23.8	14.3	9.5	4.8	
Water-Chemistry (mmol/l)										
HCO3 (mmol/l)	4.0254	3.4037	1.7254	1.6866	1.5851	1.5665	1.9206	1.6176	3.8155	1.4796
F (mmol/l)										
Cl (mmol/l)	0.0396	0.0346	0.0094	0.0092	0.0080	0.0069	0.0115	0.0090	0.0522	0.0065
NO3 (mmol/l)	0.0053	0.0609	0.0632	0.0646	0.0633	0.0631	0.0677	0.0607	0.0478	0.0611
SO4 (mmol/l)	0.0012	0.1170	0.0374	0.0356	0.0330	0.0332	0.0386	0.0436	0.2683	0.0320
Al (mmol/l)	0.0022	0.0019	0.0012	0.0011	0.0011	0.0011	0.0014	0.0012	0.0021	0.0011
Ba (mmol/l)	0.0006	0.0002	0.0002	0.0002	0.0002	0.0002	0.0002	0.0002	0.0003	0.0002
Ca (mmol/l)	1.7418	1.5435	0.7828	0.7637	0.6900	0.6879	0.8552	0.6905	1.8013	0.6579
Fe (mmol/l)	0.2689	0.0001	0.0000	0.0000	0.0000	0.0000	0.0000	0.0001	0.0000	0.0000
K (mmol/l)	0.0198	0.0208	0.0095	0.0097	0.0070	0.0088	0.0086	0.0089	0.0249	0.0074
Li (mmol/l)	0.0002	0.0003	0.0001	0.0001	0.0001	0.0001	0.0001	0.0001	0.0004	0.0001
Mg (mmol/l)	0.2984	0.3186	0.1452	0.1407	0.1315	0.1333	0.1383	0.1431	0.4921	0.1318
Na (mmol/l)	0.0567	0.0841	0.0314	0.0310	0.0260	0.0275	0.0324	0.0273	0.0811	0.0252
P (mmol/l)	0.0031	0.0029	0.0025	0.0023	0.0025	0.0026	0.0024	0.0025	0.0023	0.0024
Si (mmol/l)	0.1300	0.0968	0.0676	0.0672	0.0644	0.0644	0.0731	0.0638	0.0961	0.0617
Sr (mmol/l)	0.0017	0.0021	0.0008	0.0008	0.0007	0.0007	0.0008	0.0008	0.0031	0.0007
S (mmol/l)	0.0228	0.1213	0.0465	0.0433	0.0423	0.0409	0.0506	0.0519	0.2803	0.0400
Isotopes										
$\delta^{18}O$ (‰ VSMOW)	-11.45	-11.32	-12.05	-12.22	-12.16	-12.25	-11.91	-12.32	-11.64	-12.36
$\delta^{2}H$ (‰ VSMOW)	-79.81	-79.4	-83.7	-83.9	-83.8	-84.7	-83.1	-84.0	-80.0	-83.6
$\delta^{13}C$ (‰ VSMOW)										

Table A-7: Field data, water chemistry and isotopes at the given date ordered by outlet number.

8.6.15										
Outlet	#0	#1	#2	#3	#4	#5	#6	#7	#8	#9
Field data										
Electric cond. (µS/cm)	358	368	273	361	220	206	200	189	400	189
Temperature (°C)	7.6	7.3	6.7	7.4	6.4	6.3	6.3	6.2	7.5	6.3
pH-Value (-)	7.67	7.69	7.72	7.73	7.91	7.94	7.94	7.98	7.64	7.94
Oxygen sat. (mg/l)	8.35	8.52	10.16	8.666	10.51	10.72	10.75	10.59	8.92	10.48
Discharge (%)	16.7		33.3		8.3	16.7	8.3	8.3	8.3	
Water-Chemistry (mmol/l)										
HCO3 (mmol/l)	3.5303	3.5979	2.7912	3.4776	2.2381	2.1438	2.1261	1.9650	3.7775	1.7980
F (mmol/l)										
Cl (mmol/l)	0.0381	0.0405	0.0249	0.0381	0.0150	0.0137	0.0134	0.0127	0.0546	0.0087
NO3 (mmol/l)	0.0623	0.0641	0.0610	0.0606	0.0541	0.0581	0.0522	0.0516	0.0571	0.0105
SO4 (mmol/l)	0.1465	0.1470	0.0911	0.1297	0.0551	0.0485	0.0498	0.0566	0.2214	0.0450
Al (mmol/l)	0.0019	0.0020	0.0017	0.0019	0.0015	0.0014	0.0014	0.0013	0.0021	0.0012
Ba (mmol/l)	0.0003	0.0003	0.0003	0.0003	0.0003	0.0002	0.0002	0.0002	0.0003	0.0002
Ca (mmol/l)	1.6998	1.6837	1.2923	1.6112	1.0754	0.9643	0.9776	0.8430	1.7298	0.7810
Fe (mmol/l)	0.0001	0.0000	0.0000	0.0000	0.0000	0.0000	0.0000	0.0000	0.0000	0.0000
K (mmol/l)	0.0222	0.0228	0.0168	0.0215	0.0125	0.0117	0.0132	0.0114	0.0241	0.0095
Li (mmol/l)	0.0003	0.0003	0.0002	0.0003	0.0002	0.0001	0.0001	0.0001	0.0004	0.0001
Mg (mmol/l)	0.3585	0.3733	0.2615	0.3345	0.1921	0.1637	0.1673	0.1762	0.4823	0.1595
Na (mmol/l)	0.0898	0.0891	0.0641	0.0861	0.0492	0.0406	0.0403	0.0363	0.0784	0.0333
P (mmol/l)	0.0017	0.0019	0.0021	0.0016	0.0019	0.0021	0.0020	0.0021	0.0022	0.0020
Si (mmol/l)	0.0993	0.0982	0.0908	0.1010	0.0866	0.0837	0.0823	0.0780	0.0936	0.0777
Sr (mmol/l)	0.0023	0.0024	0.0016	0.0022	0.0012	0.0010	0.0010	0.0011	0.0031	0.0009
S (mmol/l)	0.1976	0.2043	0.1395	0.1861	0.0874	0.0780	0.0789	0.0877	0.3040	0.0755
Isotopes										
$\delta^{18}O$ (‰ VSMOW)	-11.42	-11.52	-11.63	-11.52	-11.78	-11.73	-11.80	-11.93	-11.60	-11.97
$\delta^{2}H$ (‰ VSMOW)	-80.8	-80.6	-81.4	-80.2	-81.6	-82.0	-82.7	-83.5	-82.5	-84.3
$\delta^{13}C$ (‰ VSMOW)	-12.22	-12.05	-11.51	-12.04	-10.57	-10.3	-10.61	-9.95	-12.17	-9.39

Table A-8: Field data, water chemistry and isotopes at the given date ordered by outlet number.

12.7.15										
Outlet	#0	#1	#2	#3	#4	#5	#6	#7	#8	#9
Field data										
Electric cond. (µS/cm)	372		329		266	250	227	257	386	213
Temperature (°C)	7.3		7.1		6.7	6.7	6.5	6.8	7.5	6.5
pH-Value (-)	7.7		7.72		7.83	7.87	7.92	7.86	7.67	7.89
Oxygen sat. (mg/l)	8.38		9.73		10.05	10.28	10.48	10.31	8.79	10.16
Discharge (%)	14.3		21.4		9.5	17.9	14.3	10.7	11.9	
Water-Chemistry (mmol/l)										
HCO3 (mmol/l)	3.6018		3.2702		2.6242	2.4179	2.2487	2.5064	3.7044	1.8942
F (mmol/l)										
Cl (mmol/l)	0.0471		0.0423		0.0234	0.0180	0.0144	0.0207	0.0585	0.0126
NO3 (mmol/l)	0.0644		0.0588		0.0593	0.0591	0.0568	0.0584	0.0530	0.0507
SO4 (mmol/l)	0.1634		0.1411		0.0791	0.0633	0.0576	0.0766	0.1895	0.0581
Al (mmol/l)	0.0020		0.0019		0.0016	0.0015	0.0015	0.0016	0.0020	0.0014
Ba (mmol/l)	0.0003		0.0003		0.0003	0.0003	0.0003	0.0003	0.0003	0.0003
Ca (mmol/l)	1.6278		1.5354		1.2158	1.1375	1.0832	1.1893	1.6818	0.9228
Fe (mmol/l)	0.0000		0.0000		0.0000	0.0000	0.0000	0.0000	0.0001	0.0000
K (mmol/l)	0.0219		0.0211		0.0148	0.0137	0.0130	0.0127	0.0240	0.0116
Li (mmol/l)	0.0003		0.0003		0.0002	0.0002	0.0002	0.0002	0.0003	0.0001
Mg (mmol/l)	0.3676		0.3471		0.2318	0.2025	0.1826	0.2178	0.4630	0.1894
Na (mmol/l)	0.0815		0.0734		0.0566	0.0498	0.0412	0.0483	0.0786	0.0392
P (mmol/l)	0.0019		0.0019		0.0018	0.0016	0.0018	0.0022	0.0016	0.0022
Si (mmol/l)	0.0986		0.0948		0.0909	0.0897	0.0865	0.0897	0.0927	0.0834
Sr (mmol/l)	0.0024		0.0021		0.0014	0.0012	0.0011	0.0013	0.0030	0.0011
S (mmol/l)	0.2234		0.1960		0.1239	0.1018	0.0927	0.1199	0.2846	0.0965
Isotopes										
$\delta^{18}O$ (‰ VSMOW)	-11.61		-11.57		-11.60	-11.62	-11.64	-11.63	-11.66	-11.79
$\delta^{2}H$ (‰ VSMOW)	-82.6		-82.7		-82.6	-82.6	-82.9	-82.2	-82.6	-83.1
$\delta^{13}C$ (‰ VSMOW)										

Table A-9: Field data, water chemistry and isotopes at the given date ordered by outlet number.

10.9.15										
Outlet	#0	#1	#2	#3	#4	#5	#6	#7	#8	#9
Field data										
Electric cond. (µS/cm)	368		323		272	238	205	218	382	216
Temperature (°C)	7.2		7		6.8	6.7	6.5	6.7	7.2	6.6
pH-Value (-)	7.67		7.7		7.78	7.86	7.95	7.95	7.62	7.88
Oxygen sat. (mg/l)										
Discharge (%)	14.7		19.1		7.4	19.1	16.2	13.2	10.3	
Water-Chemistry (mmol/l)										
HCO3 (mmol/l)	3.6075		3.3950		2.7533	2.3939	2.2465	2.1107	3.7376	2.0973
F (mmol/l)										
Cl (mmol/l)	0.0515		0.0426		0.0274	0.0188	0.0154	0.0129	0.0452	0.0133
NO3 (mmol/l)	0.0885		0.0545		0.0604	0.0568	0.0552	0.0512	0.0453	0.0527
SO4 (mmol/l)	0.1522		0.1464		0.0783	0.0593	0.0573	0.0652	0.2058	0.0557
Al (mmol/l)	0.0022		0.0020		0.0019	0.0017	0.0016	0.0014	0.0021	0.0014
Ba (mmol/l)	0.0002		0.0002		0.0003	0.0002	0.0002	0.0002	0.0003	0.0002
Ca (mmol/l)	1.6114		1.5199		1.2250	1.0672	1.0492	0.9308	1.6607	0.9012
Fe (mmol/l)	0.0001		0.0000		0.0000	0.0001	0.0001	0.0001	0.0001	0.0000
K (mmol/l)	0.0192		0.0172		0.0118	0.0105	0.0101	0.0092	0.0191	0.0092
Li (mmol/l)										
Mg (mmol/l)	0.3323		0.3332		0.2241	0.1998	0.2001	0.2127	0.4204	0.1917
Na (mmol/l)	0.0821		0.0753		0.0585	0.0502	0.0467	0.0448	0.0798	0.0463
P (mmol/l)										
Si (mmol/l)	0.0977		0.0926		0.0911	0.0875	0.0862	0.0838	0.0910	0.0818
Sr (mmol/l)	0.0023		0.0022		0.0014	0.0012	0.0012	0.0012	0.0029	0.0011
S (mmol/l)	0.1608		0.1543		0.0928	0.0755	0.0783	0.0775	0.2246	0.0690
Isotopes										
$\delta^{18}O$ (‰ VSMOW)										
$\delta^{2}H$ (‰ VSMOW)										
$\delta^{13}C$ (‰ VSMOW)										

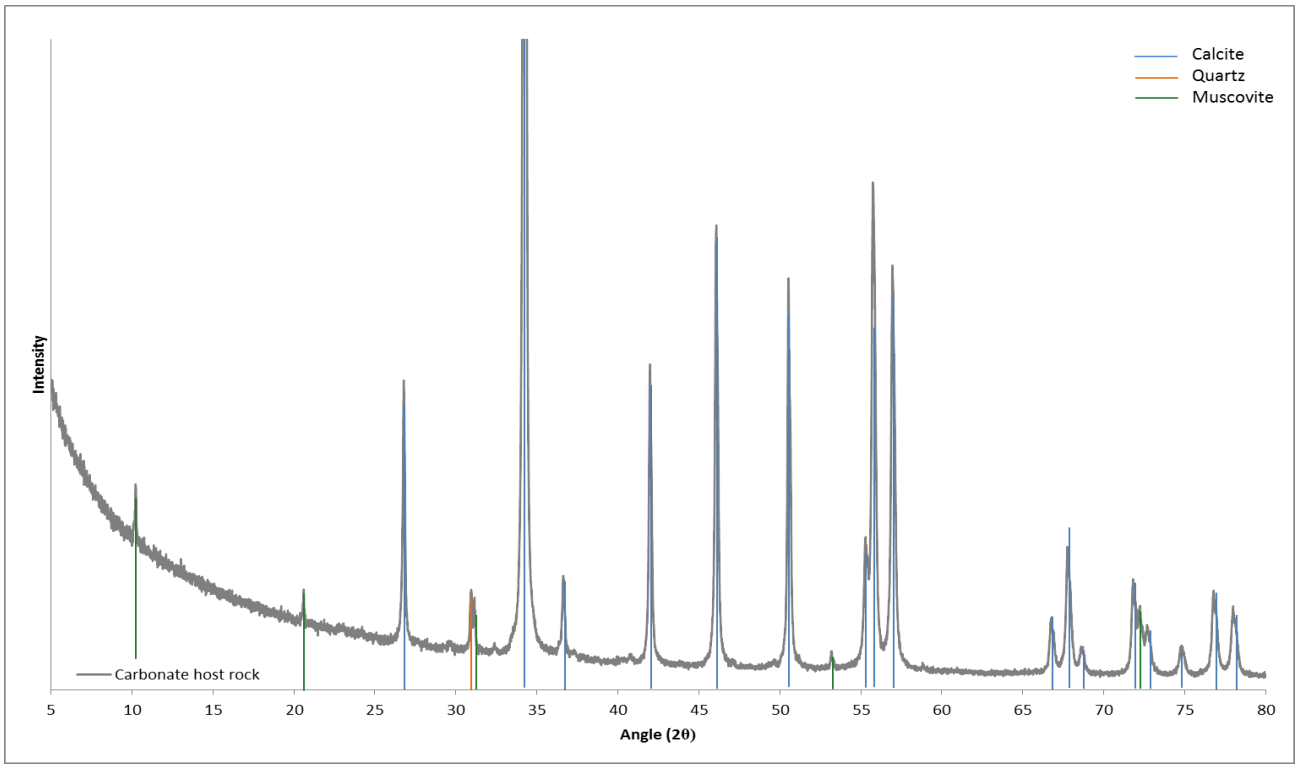

Figure A-1 XRD-Analysis of the carbonate host rock. Sample was taken 50 m east of the uranin tracer test location (s. Figure 2-1).

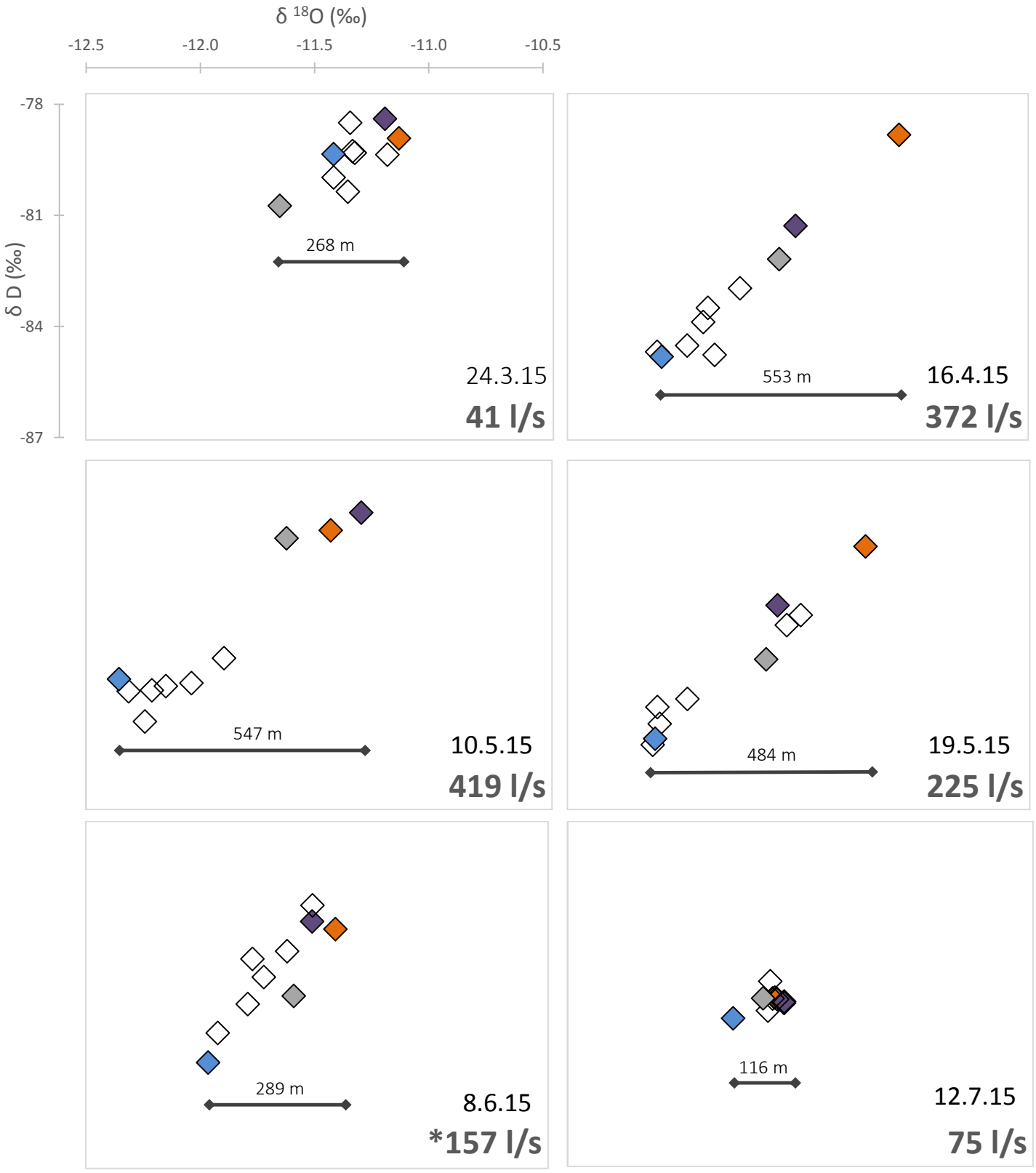

Figure A-2 Plot for the water isotopes D and ^{18}O organized after datum of fieldtrip. The at the time discharge value is display in the bottom right corner. The black bars below each sample set displays the range of δ ^{18}O values used for calculating the altitude difference between the samples as shown above the bar. Color scheme: #0 (orange), #1 (purple), #2-#7 (light grey), #8 (dark grey), #9 (blue).

k

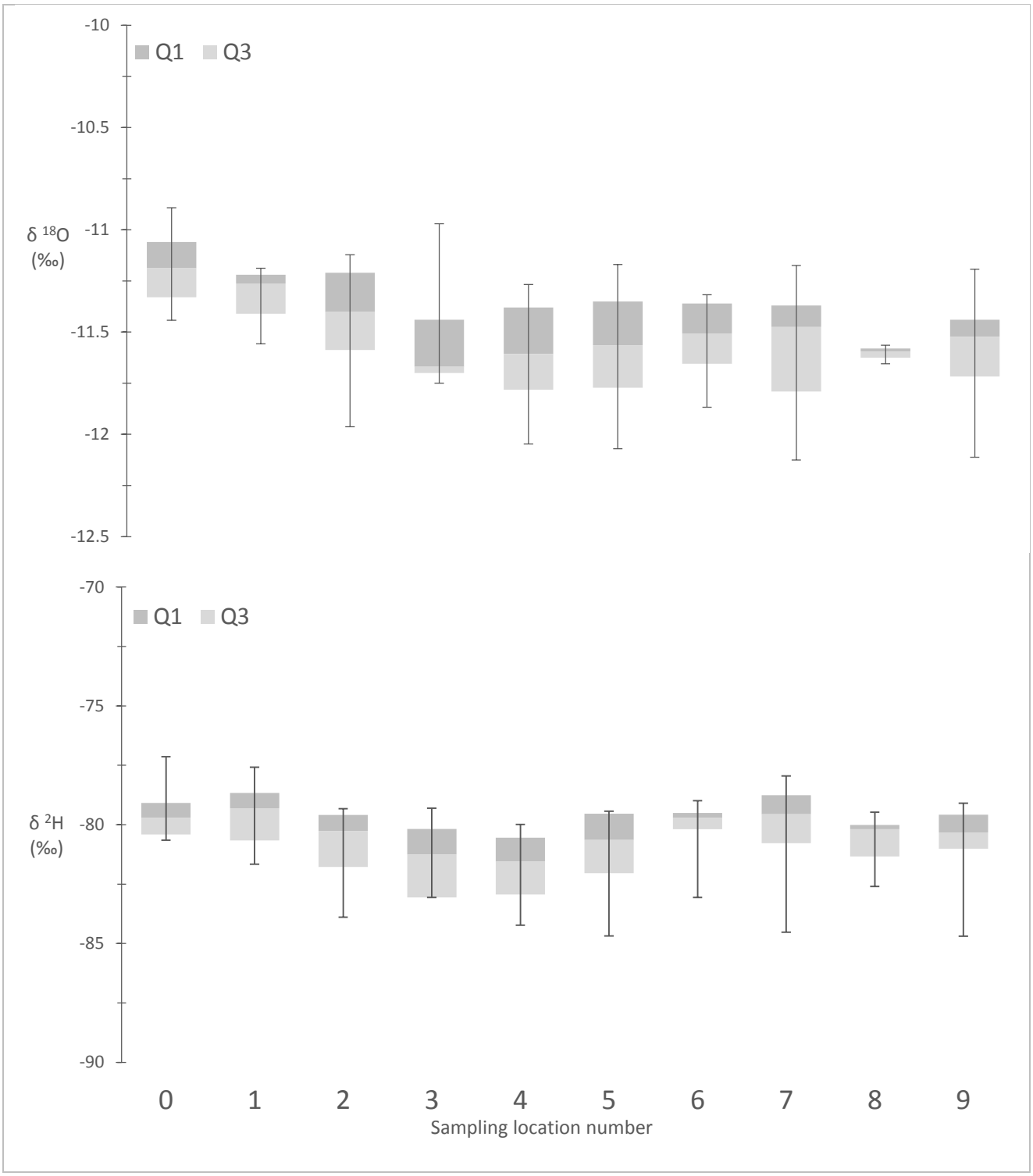

Figure A-3: Boxplots showing the statistical variance for Oxygen-18 and Deuterium isotopes of the respective sampling locations for all water samples over time. The dark and light grey boxes mark the borders from quartile 1 (25 %) to quartile 3 (75 %).

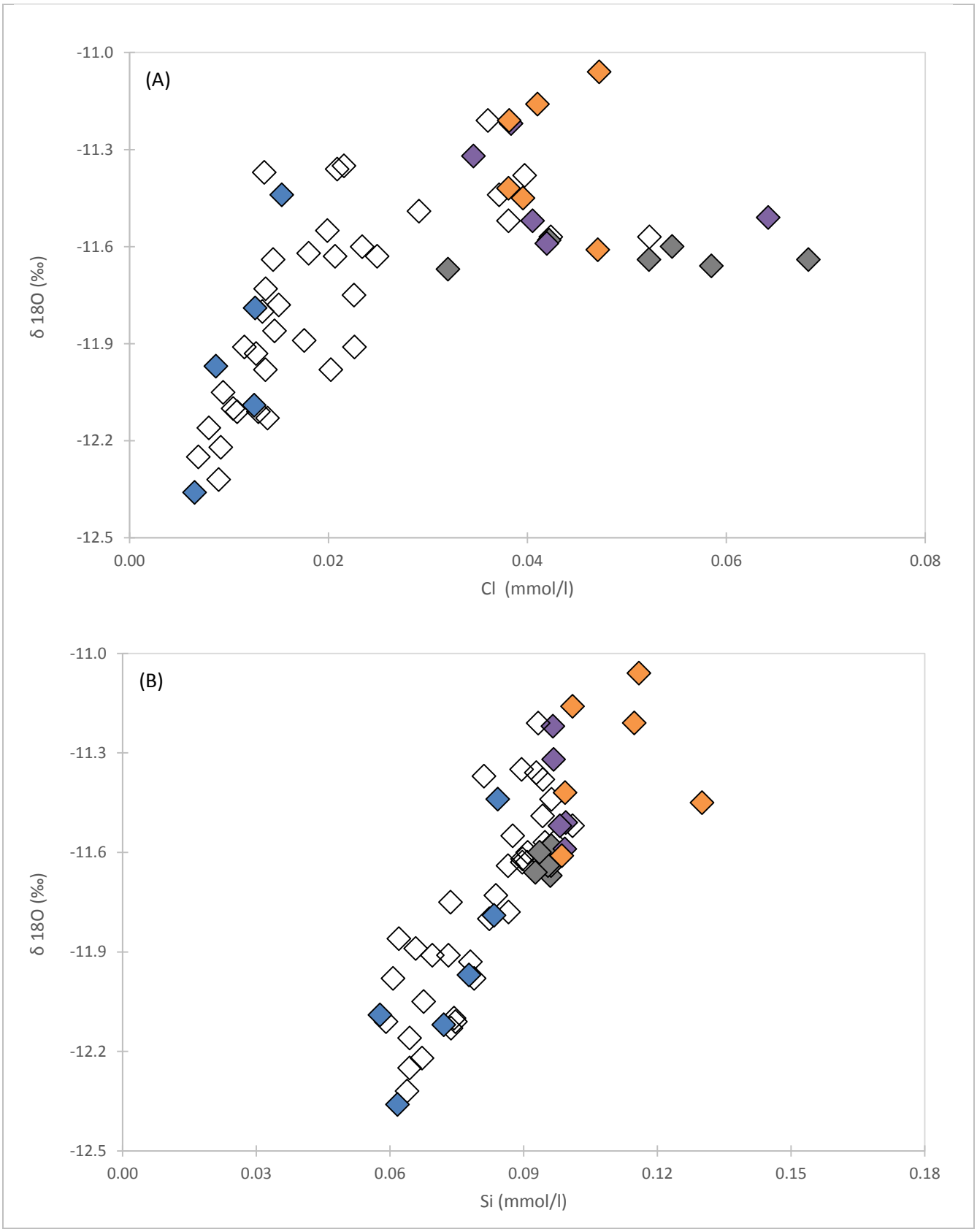

Figure A-4: (A) Plot of δ ^{18}O vs chloride concentration and (B) plot of δ ^{18}O vs silica. Color scheme: #0 (orange), #1 (purple), #2-#7 (white), #8 (dark grey), #9 (blue).

m